

Snowball Earth: Ice thickness on the tropical ocean

Stephen G. Warren¹, Richard E. Brandt¹, Thomas C. Grenfell¹,
and Christopher P. McKay²

¹Department of Atmospheric Sciences, University of Washington, Seattle, Washington

²Space Science Division, NASA Ames Research Center, Moffett Field, California

Submitted to *Journal of Geophysical Research (Oceans)*, August 2001

Revised 30 May 2002

Abstract. On the tropical oceans of a Neoproterozoic Snowball Earth, snow-free ice would have existed in regions of net sublimation. Photosynthesis could have continued beneath this bare ice if it was sufficiently thin and sufficiently clear. The steady-state ice thickness is determined by the necessity to balance the upward conduction of heat with three subsurface heating rates: the heat flux from the ocean to the ice base, the latent heat of freezing to the ice base, and the solar energy absorbed within the ice. A preliminary study, using a broadband model for solar radiation and assuming a large freezing rate, had indicated that tropical ice might be only a few meters thick. Here we show that the vertical throughput of ice by surface sublimation and basal freezing would be too slow to keep the ice thin, and that the broadband model had exaggerated the absorption depth of sunlight. We use a spectral model for solar absorption, computing radiative transfer at 60 wavelengths, considering absorption by the ice and scattering by bubbles. With the spectral model the computed ice thickness is much greater. For a solar flux of 320 W m^{-2} at the equatorial surface, and expected albedo of 0.5 for bare sea ice, we find that surface temperatures below -12°C generate ice layers too thick for photosynthesis ($>100\text{m}$). If the albedo were as low as 0.4, thick ice would occur only for surface temperatures below -25°C , but such low temperatures would be difficult to maintain with such low albedo. For surface temperatures warmer than these limits the ice becomes thin ($<1\text{m}$) and is unlikely to represent a coherent ice layer. However, glacial deformation of thick floating ice from nearby oceanic regions may preclude the existence of thin or ice-free patches.

1. Introduction

Geological evidence of glaciers extending to sea level at low latitude in the Neoproterozoic period about 700 Million years (Myr) ago was first presented by *Harland* [1964] and recently reviewed by *Evans* [2000]. Energy-balance climate modeling of the snow-albedo feedback [*Budyko*, 1969; *Sellers*, 1969] indicated that if sea ice reaches 30 degrees latitude it will proceed catastrophically to the equator. *Kirschvink* [1992] drew the connection between the geological evidence and climate modeling to propose that the Earth had indeed been entirely ice-covered on at least two occasions during the Neoproterozoic. That hypothesis was greatly strengthened by carbon-isotopic evidence from carbonate sedimentary rocks [*Hoffman et al.*, 1998]. Climate models of the greenhouse effect from volcanic CO₂ [*Caldeira and Kasting*, 1992], and geological evidence from thickness of the carbonate layers [*Hoffman et al.*, 1998; *Hoffman and Schrag*, 2000], both suggest that the ice-covered state persisted for 4-30 Myr. The suggested cause of the snowball events was a reduction of the atmospheric greenhouse effect resulting from disturbance to the global carbon cycle that affected levels of both CO₂ and CH₄ [*Schrag et al.*, 2002].

Photosynthetic eukaryotic algae appear to have been present both before and after the times of the hypothesized snowball events [*Knoll*, 1985]. They could have survived either in isolated pools of liquid water at the surface at geothermal hotspots such as in Iceland today [*Hoffman and Schrag*, 2000], or as a widespread community under thin snow-free sea ice in a tropical oceanic belt of net sublimation [*McKay*, 2000]. Survival only at isolated hotspot refugia could have promoted the evolution of diversity and might

help to explain the ‘Cambrian Explosion’ (the simultaneous appearance of many animal phyla) 575-525 Myr ago that followed the snowball events.

Here we examine the second possibility, that sunlight adequate for photosynthesis could be transmitted through the sea ice. Where the ice was snow-covered, its equilibrium thickness (after the ocean had lost its reservoir of heat) would have been at least several hundred meters, and probably over a kilometer; here we investigate whether the ice might have been thin in snowfree regions. According to the GENESIS general circulation model [Pollard and Kasting, 2001; Pollard, personal communication, 2001], in nearly half the modern ocean, mostly in subtropical bands centered at 20°N and 20°S, evaporation (E) exceeds precipitation (P), typically by 1-5 mm/day. The same climate model applied to Snowball Earth conditions at 750 Myr ago and 550 Myr ago similarly indicates that about half the world ocean had negative $P-E$, but in a single belt centered on the Equator rather than in two subtropical belts, and with net sublimation rates of only 1-10 mm/year. These are conditions for “full snowball,” the coldest part of the snowball era before CO₂ had risen substantially.

The snowball hypothesis; i.e., that the ocean surface completely froze, is not universally accepted [Kennedy *et al.*, 2001; Williams and Schmidt, 2000]. Here we examine consequences of the hypothesis, which may prove useful in testing its validity. In this paper we assume that the snowball events did occur, and we compute the ice thicknesses that would have resulted, given a range of boundary conditions. We assume that the surface temperatures were below 0°C over the entire Earth in all seasons. An initial investigation of the thickness of tropical sea ice was made by McKay [2000]; in this paper we obtain improved estimates.

2. Heat conduction model for ice thickness

Thermodynamic models of equilibrium sea-ice thickness [e.g. *Maykut and Untersteiner, 1971*] typically consist of (a) a surface energy budget to determine the surface temperature T_s , (b) a bottom energy budget to determine the freezing rate and associated latent heat release F_L , and (c) an equation for heat conduction through the ice. *McKay* [2000] reduced the problem to a single equation (the heat-conduction equation), by specifying T_s and F_L :

$$k \frac{dT}{dz} = S(z) + F_L + F_g, \quad (1)$$

where k is the thermal conductivity of ice, T is the mean annual temperature at depth z below the ice surface, $S(z)$ is the solar radiation flux absorbed below level z , and F_g is the geothermal heat flux supplied to the base of the ice. The three terms on the right-hand side are the three sources of heat that must be balanced by the heat conducted upward across level z . During a transient period following the initial freezing of the tropical ocean surface, the heat supplied by the ocean water to the base of the ice would have exceeded F_g ; Eq. 1 applies to the equilibrium situation that becomes established after the ocean has lost its reservoir of heat. (The transient period would be short. Even if the entire depth of the ocean has to cool by 10 K at the rate of only 1 W m^{-2} , the transient period would be only 5000 years. Maximum modern heat fluxes from ocean to atmosphere are over the Gulf Stream in autumn, 400 W m^{-2} [*Sellers, 1965, Figure 32*]. A flux of 1 W m^{-2} can be conducted through 70 m of ice with $T_s = -30^\circ\text{C}$.)

For snow-covered ice, essentially all the absorbed sunlight is absorbed in the top few centimeters [*Brandt and Warren, 1993*], resulting in very thick ice. This is why lakes under the snow-covered East Antarctic ice sheet occur only under thick ice. The

existence of Lake Vostok (and the nonexistence of lakes under thin parts of the ice sheet) is consistent with Eq. 1 if $S(z)$ is set to zero and F_L is small. For $F_g = 0.035 \text{ W m}^{-2}$, $F_L = 0$, $k = 2.5 \text{ W m}^{-1}\text{K}^{-1}$, $T_s = -55^\circ\text{C}$, and ice thickness $Z = 3700 \text{ m}$ [Kapitsa *et al.*, 1996], Eq. 1 gives bottom temperature $T_o = -3.4^\circ\text{C}$, the freezing point of water under 340 bars pressure.

By contrast, the ice cover of Lake Hoare, in the McMurdo Dry Valleys at the same latitude as Lake Vostok (78°S), is thinner by three orders of magnitude ($Z = 5\text{m}$). Higher T_s (-20°C) and greater F_g (0.08 W m^{-2}) together account for only a factor of 6 difference in ice thickness; the major heat fluxes responsible for the thinness of the lake ice are latent heat released by freezing of lakewater to the bottom of the ice, and penetration of solar radiation into the ice, as explained by *McKay et al.* [1985].

McKay [2000] used Lake Hoare as a surrogate for sea ice on the Snowball Ocean, with $F_L = 3.4 \text{ W m}^{-2}$ (corresponding to a freezing rate of 35 cm/year). Strong dry winds cause 35 cm/year of sublimation from the surface of Lake Hoare; the ice thickness is maintained in a steady state by freezing of lakewater to the base at the same rate. This water is supplied by meltwater from a nearby glacier; the water flows under the ice when a moat forms at the edge of the lake in summer. Recent climate modeling results for Snowball Earth, however, show that Lake Hoare is an inappropriate surrogate as regards latent-heat release.

The climate-model estimates of $P-E$ from *Pollard and Kasting* [2001] and Pollard (personal communication), cited above, imply a freezing rate at the base of tropical sea ice of $1\text{-}10 \text{ mm/year}$, corresponding to a latent heat release at the base of only $0.01\text{-}0.10 \text{ W m}^{-2}$; i.e., the same order of magnitude as F_g . Furthermore, even this small amount of

latent heat of fusion that is released at the base of the ice need not be conducted upward through the ice; it may instead be transferred horizontally via the "ice pump" mechanism that occurs under ice shelves, making use of the pressure-dependence of freezing temperature [Lewis and Perkin, 1986; Kipfstuhl et al., 1992]. For example, seawater freezes to the base of the Amery Ice Shelf in East Antarctica at a rate of 20 cm/year [Morgan, 1972; Budd et al., 1982], implying $F_L = 2 \text{ W m}^{-2}$, but the ice is 400 m thick so only 0.1 W m^{-2} can be conducted upward through the ice. Most of the latent heat released is used to warm supercooled seawater up to the local freezing temperature, effectively resulting in a horizontal transfer of heat to deeper parts of the ice-shelf base. The relevance of the ice pump to Snowball Earth is uncertain, because the slope of the ice bottom would have been much less than on modern ice shelves.

In any case, the geothermal heat flux and the latent heat flux would both be of small magnitude in the snowball ocean, of order $0.01\text{-}0.1 \text{ W m}^{-2}$. Their exact values do become important in determining the ice thickness if it is in the range 300-3000 m, but they cannot cause the ice to be thin. On the other hand, the incident solar radiation S_o at the equatorial sea surface is on the order of 300 W m^{-2} (averaged over day and night), so if even a small part of this energy can be absorbed at depth in the ice it completely overwhelms F_L and F_g in determining ice thickness, and offers the possibility of thin ice even with low surface temperatures. We therefore now take particular care to compute the vertical distribution of absorbed sunlight accurately.

3. Model of solar radiation absorption

Integration of (1) yields

$$k\Delta T = Z(F_g + F_L) + \int_0^Z S(z)dz, \quad (2)$$

where $\Delta T \equiv T_o - T_s$, the temperature difference from bottom to top, and Z is the total ice thickness to be solved for. Here we assume $k = 2.4 \text{ W m}^{-1}\text{K}^{-1}$ independent of depth. The thermal conductivity of ice varies from 2.2 at 0°C to 2.7 at -40°C , and *McKay* [2000] accounted for this temperature dependence; here we use a constant value of k for simplicity. The error in Z caused by this approximation is small compared to uncertainty in Z caused by lack of knowledge of surface temperature and ice transparency.

McKay [2000] expressed $S(z)$ as a single exponential function:

$$S(z) = S_0(1 - \alpha)\exp(-z/h), \quad (3)$$

where S_0 is the solar flux incident on the top surface, α is the albedo, and h is the attenuation length for absorption, $h = 0.8 \text{ m}$. In reality, both α and (more importantly) h depend on wavelength; we now show that the assumption of constant h (i.e. the “broadband” approximation) deposits the absorbed solar energy too deeply in the ice. In reality the wavelengths that are absorbed by ice (near-infrared) are absorbed near the surface, and the wavelengths that do penetrate (visible) are mostly not absorbed; they are turned around by scattering off air bubbles, vapor bubbles, and brine inclusions, and re-emerge to contribute to the albedo.

We use $n = 50$ vertical layers and $l = 60$ wavelength intervals to compute radiative transfer in the ice. For level j at depth z_j , instead of (3) we use:

$$S(z_j) = \sum_{i=j}^n f_i + f_{n+1}, \quad (4)$$

where f_i is the solar flux absorbed in layer i within the ice (each f_i is a sum over 60 wavelength intervals) and f_{n+1} is the solar flux absorbed in the water below the ice. Eq. 2 then becomes

$$k\Delta T = Z(F_g + F_L + f_{n+1}) + \sum_{i=1}^n i f_i \Delta z_i. \quad (5)$$

The factor i appears in the summation in (5) because $S(z)$ in (2) is itself an integral (Eq. 4); the energy of solar absorption at *all* levels below level i must be conducted upward across level i .

3.1. Absorption spectrum of ice

Figure 1 shows that the spectral absorption coefficient of ice (the reciprocal of the attenuation length) varies by 6 orders of magnitude across the solar spectrum, and compares it to the single value of h^{-1} used in the earlier work. Ice absorbs most weakly in the blue and near-ultraviolet parts of the spectrum. The solid line in Figure 2 comes mostly from *Warren's* [1984] compilation of laboratory measurements; for the visible and near-visible wavelengths (0.3-1.4 μm) the absorption was determined by measuring attenuation of a beam passing through clear bubble-free ice [*Grenfell and Perovich, 1981; Perovich and Govoni, 1991*]. If a small amount of undetectable scattering was present, the reported absorption coefficient k_{abs} would be too large. Recently, measurements of photon travel-time distributions in ice by the Antarctic Muon and Neutrino Detector Array (AMANDA) have been used to infer both scattering and absorption coefficients [*Price and Bergström, 1997; Askebjør et al., 1997a,b; K. Woschnagg, 2002, personal communication*]. The AMANDA absorption coefficients agree with the laboratory measurements at wavelengths $\lambda > 0.6 \mu\text{m}$, but at shorter wavelengths AMANDA infers a smaller k_{abs} than

obtained in the laboratory, suggesting that the laboratory ice did indeed exhibit a small amount of scattering; this scattering dominated the absorption at blue wavelengths because the absorption is so weak there.

The absorption by ice is so weak in the visible and ultraviolet (UV) that k_{abs} in Antarctic ice is dominated by the small amount of dust naturally present in the ice. The k_{abs} is higher in ice that fell as snow during the last glacial maximum, when the atmosphere was dustier [He and Price, 1998]. Our calculations in this paper use k_{abs} for the cleanest ice at the South Pole (dashed line in Figure 1). The ice in the snowball tropics is likely to have contained more dust than this cleanest ice, because it would have collected windblown dust from unglaciated continental deserts. The equilibrium ice thickness Z given by (5) is smaller if k_{abs} is smaller, because sunlight penetrates more deeply, so by using the dashed line in Figure 1 we are biasing our results toward thin ice. We can therefore be confident in the conclusion of our model if it predicts thick ice.

3.2. Incident solar radiation spectrum

To obtain the incident solar spectrum at sea level, we have taken the subarctic summer (SAS) standard atmosphere of McClatchey *et al.* [1972] and multiplied the temperatures at all levels by the factor 0.812, so as to obtain a surface air temperature $T_s = -40^\circ\text{C}$. We used the SAS atmosphere as a starting point, rather than the subarctic winter (SAW) because the SAW contains a surface-based temperature inversion that we think is unlikely to have been present under the intense sunlight at low latitudes. For the water vapor content of the modified SAS atmosphere we assumed saturation with respect to ice up to 10 km; dry above. We then used an atmospheric radiation model, “ATRAD”

[Wiscombe *et al.*, 1984], to compute the spectral downward flux at the sea surface under clear sky (Figure 2). In comparison to the spectrum for the unmodified SAS atmosphere (dashed line in Figure 2), the cold atmosphere absorbs much less radiation in the water-vapor bands.

The reason we assumed saturation with respect to ice was that this is what is commonly found in the troposphere over the Antarctic Plateau, where the surface temperature is similar to that of the snowball tropics. This assumption of saturation probably exaggerates the relative humidity of the tropical troposphere. However, the water-vapor content of an atmosphere at -40°C with 100% relative humidity is the same as that of an atmosphere at -30°C with 34% relative humidity, so the solar spectrum we are using should be appropriate for the standard case below, where $T_s = -30^{\circ}\text{C}$.

3.3. Radiative transfer in ice

The ice in this model has a clean top surface; it is free of any deposits of snow, salt, or dust. The ice is assumed to be homogeneous and contains a uniform distribution of spherical air bubbles of radius 0.1 mm of specified number-density n_{eff} . The single-scattering phase function of the bubbles is given by *Mullen and Warren* [1988]. Bubbles are used to represent all scatterers in the ice; brine inclusions are not explicitly modeled. In the marine ice discussed below, the scattering is by cracks rather than bubbles, but bubbles can adequately represent their effect on radiative transfer [cf. *Bohren*, 1983], because both bubbles and cracks are non-spectrally-selective scatterers. The fact that the spectral absorption coefficient of water is very similar to that of ice allows scattering by brine

inclusions also to be represented adequately by an effective bubble density in the model. The flat upper surface of the ice reflects specularly both up and down.

We use a multilayer discrete-ordinates radiative transfer model with a specularly-reflecting upper surface, developed by *Grenfell* [1983]. Radiation fluxes are computed at 50 unequally-spaced vertical levels (with finer spacing near the upper surface) to determine the total absorbed radiation within each layer. The model was run for twelve bubble densities, two solar zenith angles, and for ice thickness Z ranging from 0.1 m to 30 m at 0.1-m increments and from 30 m to 200 m at 1-m increments, for a total of 11,280 cases. For the thinnest cases the spacing of vertical levels increased from 0.5 mm at the top to 2.5 mm at the bottom. For $Z = 200$ m the layer spacing increased from 0.5 mm at the top to 25 m at the bottom. (For $Z > 200$ m there is no need for vertical resolution below 200 m because no sunlight penetrates that deeply.) For each of these cases the sum $\sum_i f_i \Delta z_i$ and the flux f_{n+1} to be used in Eq. 5 were computed and stored in a lookup table for computation of equilibrium ice thickness. We also ran the radiative transfer model at finer and coarser vertical resolution to ensure that the sum used for Eq. 5 had converged at all ice thicknesses. With specified surface temperature, bottom fluxes, ice bubble density, and solar zenith angle, the equilibrium ice thickness can be computed by iterating Equation 5 to solve for Z using the following method. From the lookup table, $\sum_i f_i \Delta z_i$ and f_{n+1} for 0.1-m ice is used to calculate Z . If the calculated Z exceeds 0.1 m, the next entry in the table is used, and so on, until the minimum difference between the thickness in the table entry and Z is found. If Z exceeds 200 m, the ice is optically thick even for low bubble densities so $\sum_i f_i \Delta z_i$ is the same as it would be for 200-m-thick ice (because all the solar flux is

absorbed in the top 200 m) and $f_{n+1} = 0$ (no solar flux exits the bottom of the ice), so Eq. 5 is now explicit and can be solved directly for Z .

Figure 3 shows the absorption of solar radiation as a function of depth in the top meter of the ice for a bubble density $n_{eff} = 10 \text{ mm}^{-3}$, corresponding to an albedo of 0.6. The broadband model, also shown in Figure 3, has the same albedo, and hence the same total absorbed energy, but the absorbed energy is distributed with depth quite differently in the two models. The near-infrared part of the solar spectrum is responsible for the high near-surface absorption rate in the spectral model. Figure 4 is an expanded view of the uppermost 1 millimeter of Figure 3, for two ice types: pure ice with no bubbles, and ice with high bubble density ($n_{eff} = 200 \text{ mm}^{-3}$), both computed using the spectral model. The broadband model's absorption in the top millimeter is so close to zero on this scale that it cannot be distinguished from the left vertical axis. Figures 3 and 4 confirm the expectation expressed above, that the broadband model deposits the solar radiation too deeply in the ice.

Figure 5 shows the spectrally averaged (“allwave”) albedo, α , for 2-m-thick ice and 200-m-thick ice as a function of bubble density for direct-beam incidence at solar zenith angle $\theta_0 = 0^\circ$ or $\theta_0 = 60^\circ$. The albedo at very low bubble content is just the Fresnel reflectivity of the surface, which depends on incidence angle. In subsequent figures we often use albedo of 200-m-thick ice as a convenient surrogate for bubble density.

Figure 6 shows the fraction of the absorbed solar flux that is absorbed in the topmost layers of ice, as a function of bubble density (bottom scale) or albedo (top scale). For albedos 0.3-0.5, 50-85% of the absorption occurs in the topmost 10 cm and is therefore quickly conducted up to the top surface. In the broadband model only 12% of the

absorption is deposited into the topmost 10 cm; the remainder penetrates more deeply and its energy must then be conducted up, resulting in an equilibrium ice thickness that is too small, as shown in Figure 7, which we discuss next.

3.4. Equilibrium ice thickness: spectral versus broadband model

Figure 7 compares the equilibrium ice thickness, Z , computed by the spectral model to that computed by the broadband model, for conditions expected to be representative of the equatorial ocean on Snowball Earth. In both cases Z is plotted as a function of albedo (a surrogate for n_{eff} , which is also shown on the top horizontal axis). This “albedo” is the asymptotic albedo for 200-m-thick ice, which is indistinguishable from the albedo of kilometer-thick ice.

Both models use $F_g = 0.08 \text{ W m}^{-2}$, a typical value for geothermal heat flux from the ocean floor [Lillie, 1999]. As discussed above, F_L is at most 0.1 W m^{-2} , and at this value it would reduce the thickness of thick ice by a factor of 2 but would not change the location of the steep transition to thin ice in Figure 7. Whatever value we choose for F_L in the range $0.0\text{-}0.1 \text{ W m}^{-2}$ will not affect our conclusions about the possible existence of thin ice. It is even possible that F_L is negative in the tropics and the ice thicker than we calculate here [Goodman and Pierrehumbert, 2002]. We therefore set $F_L = 0$ for simplicity.

For the surface temperature T_s we refer to the results of the GENESIS model [Pollard and Kasting, 2001; Pollard, personal communication], which gives $T_s = -30$ to -35°C for the equatorial ocean in all seasons in the “full snowball” state. In Figure 7 we set $T_s = -30^\circ\text{C}$. The temperature at the bottom of the ice is -2°C , the freezing point of seawater.

The solar irradiance incident at the surface, $S_0 = 320 \text{ W m}^{-2}$, is an estimate of the mean annual equatorial value for 700 Myr ago, as follows. The annual average solar flux, S_0 , incident at the surface at latitude ϕ , is given by

$$S_0(\phi) = 0.94 \left(\frac{Q_0}{4} \right) s(\phi) t, \quad (6)$$

where Q_0 is the present value of the solar constant, $Q_0 = 1370 \text{ W m}^{-2}$, $s(\phi)$ is the normalized latitudinal distribution of insolation, and t is the annual average atmospheric transmittance (average of clear and cloudy skies). The factor 0.94 accounts for the 6% reduction in solar constant expected for 700 Myr ago. For an orbital obliquity of 23.5° , the equatorial value of $s(0)$ is 1.224 [Chylek and Coakley, 1975, Table 1]. The atmospheric transmittance t given by ATRAD for the cold atmosphere (Figure 2) is $t = 0.88$ for the global average solar zenith angle $\theta_0 = 60^\circ$, and $t = 0.92$ for overhead sun, $\theta_0 = 0^\circ$. These values of t assume the atmosphere is devoid of clouds and ice crystals, which in reality would be present at times. To account for clouds and ice crystals, we use $t = 0.81$ and obtain $S_0 = 320 \text{ W m}^{-2}$. (However, in Figure 11 below we will show results for all values of S_0 in the range 0 to 400 W m^{-2} .)

Figure 7 shows that as n_{eff} increases, there is a sharp transition in ice thickness from less than 1 meter to several hundred meters. This transition occurs when the ice becomes sufficiently opaque that essentially no sunlight reaches the lower parts of the ice; then the ice thickness jumps to a large value limited only by the geothermal heat flux.

With the more accurate spectral model it is much easier to get thick ice. For any albedo in the range 0.4-0.7 the spectral model gives $Z > 200 \text{ m}$ but the broadband model gives $Z < 2 \text{ m}$. In the earlier work [McKay, 2000], the broadband model indicated that even for albedo as high as 0.7 the tropical ice could be thin enough to permit

photosynthesis below. The spectral model shows that this is impossible. We will argue in Section 4 below that bare ice would have albedo greater than 0.4 and would therefore be thick.

The lower (thin-ice) branch of the curve, below the inflection point, is probably not relevant to the real Earth. It indicates, for example, that ice with an albedo of 0.3 could have an equilibrium thickness of 0.6 m. But this result is obtained only because we have specified $T_s = -30^\circ\text{C}$. In reality an ocean albedo less than 0.4 under a tropical sun is probably inconsistent with $T_s < 0^\circ\text{C}$. When $\alpha = 0.4$ is specified for the tropical ocean in a general circulation model of Snowball Earth [D. Pollard, personal communication, 2001], the surface temperature rises to the melting point and the ice melts. We therefore have drawn a dashed line in Figure 7 to show our expectation of how the equilibrium ice thickness would likely drop to zero for low albedo in a coupled sea-ice/climate model.

Low-albedo ice does exist on the modern Earth in the Dry Valley lakes, because of the low regional air temperature. Thin ice of low albedo could possibly occur on tropical lakes on Snowball Earth, if they were sufficiently small in area that their low albedo did not affect the regional climate, so that the low regional air temperature could keep them frozen. They would have to be landlocked, because any small thin-ice regions on the sea would be invaded by glacial flow of nearby thicker ice.

3.5. The Dry Valley lakes revisited

Since the broadband model leads to large errors in the computed ice thickness for the tropical ocean, we must ask why it was able to give the correct thickness for lake ice in the McMurdo Dry Valleys, 3-6 m. Using the annual average solar incidence ($S_0 = 104$

W m^{-2}) and a latent-heat flux of 3.4 W m^{-2} , corresponding to the observed freezing rate of 35 cm/year, *McKay et al.* [1985] computed $Z = 3.4 \text{ m}$ for an allwave albedo $\alpha = 0.6$. When we put the bubble density corresponding to this albedo into the spectral model, we compute $Z = 13 \text{ m}$. It appears that the reason for the broadband model's correct prediction of thickness was the use of an unrealistically high albedo. The albedo of 0.6 used by *McKay et al.* [1985] was based on a single cursory measurement ("slightly more than 0.50") on Lake Vanda [*Ragotzkie et al.*, 1964]. However, when *McKay et al.* [1994, Figures 11, 13] measured the albedo accurately and repeatedly on Lake Hoare, it averaged to about 0.3. With this observed albedo, it is the spectral model that gives a reasonable ice thickness, $Z = 4 \text{ m}$; the broadband model makes it too thin ($Z = 1 \text{ m}$).

The simple analytical model can still be applied to the ice covers of the Dry Valley lakes if one considers it as a two-band model: a visible band that penetrates the ice cover and a near-IR band that does not. About half the solar radiation is in the visible band. Using the measured visible albedo for Lake Hoare (0.3) and computing $h = 1.2 \text{ m}$ from the measured transmissivity of the lake ice in the visible [*McKay et al.*, 1994] the model correctly predicts the ice thickness (4 m for a mean annual temperature of -20°C) when the solar flux is reduced by a factor of 2.

4. Modern surrogates for ice on the tropical ocean

In steady state, ice in the snowfree regions of the tropical ocean will experience a slow loss of a few mm per year by sublimation at the upper surface, balanced by freezing of seawater at the lower surface and inflow from higher latitudes where the ice is thicker. The kilometer-thick snow-covered ice sheets covering midlatitude and polar oceans would

flow like modern ice shelves, but we prefer to call them “sea-glaciers” because their existence is independent of any continental glaciation. Near the poleward limit of the net-sublimation region the bare ice will therefore be freshwater ice (resembling glacier ice), originally formed by compression of snow, that has flowed equatorward as sea-glaciers [Goodman and Pierrehumbert, 2002]. Closer to the equator, if the net sublimation rate exceeds the rate of net ice inflow, the ice exposed at the surface will consist of frozen seawater. There are therefore several modern ice types that should be considered as possible surrogates for ice on the tropical ocean, all of which are more appropriate than the lake ice of the Dry Valleys. They are summarized in Table 1.

4.1. Glacier ice

In some mountainous regions in Antarctica, strong winds blow away the fallen snow, exposing areas of glacier ice, which are further ablated by sublimation. The spectral albedo of this ice was measured at one site by Warren *et al.* [1993a] and is shown in Figure 8; the allwave albedo at several sites has been reported by Bintanja [1999], averaging 0.6. The exposed surface is often called “blue ice,” but its appearance might better be described as “blue-white,” because the ice contains numerous bubbles, since the origin of this ice was compression of snow.

4.2. Frozen seawater

On regions of the snowball ocean where net sublimation exceeds inflow of sea-glaciers, seawater will freeze to the base. The density of bubbles (and brine inclusions) incorporated into this ice will depend on the rate of freezing and also on the depth at which

freezing occurs; i.e., on how thick the ice is. These bubbles and brine inclusions will then be carried slowly upward as the top surface sublimates. Both bubbles and brine inclusions migrate toward the warm end of a temperature gradient [Wettlaufer, 1998], but the sublimation rate probably exceeds the migration rate [Warren *et al.*, 2002]. This process can lead to accumulation of salt crystals at the top surface, as discussed below, but for now we ignore the possibility of a salt crust.

Three modern examples of frozen seawater can serve as surrogates. The first is sea ice freezing at the ocean surface. Such ice that has grown through an entire winter is normally snow-covered, but near the coast of Antarctica strong winds blow the snow away. The spectral albedo of bare cold sea ice, 1.4 m thick, measured by *Brandt et al.* [1999], is shown in Figure 8. Its allwave albedo was 0.49 under the ambient conditions, but it would be lower, about 0.47, under the colder atmosphere of Snowball Earth, because the near-infrared solar radiation, for which ice has low albedo, would not be filtered out as effectively by atmospheric water vapor (Table 1). Figure 8 also shows the dramatic effect of a thin layer of snow, which was found in patches on this same region of coastal ice. Just 5-10 mm of snow raised the albedo from 0.49 to 0.81.

That ice was measured at a temperature of -5°C . If it had been much colder, below the eutectic temperature of NaCl in seawater, -23°C [Pounder, 1965], salt crystals forming in the brine inclusions would have raised the albedo. Such sub-eutectic ice has been studied only in the laboratory, by *Perovich and Grenfell* [1981], who measured spectral albedo from 400 to 1000 nm. This wavelength range covers about 80% of the solar energy spectrum. We extrapolate the measured spectral albedo further into the near-infrared using spectral shapes of albedo that are typical of sea ice (a procedure used previously by *Allison*

et al. [1993]) and obtain an estimated allwave albedo $\alpha = 0.75$ under the subarctic summer atmosphere, and 0.71 under the cold atmosphere (Figure 8, Table 1). The albedo of bare ice on the equator of Snowball Earth will reach this level only if $T_s < -23^\circ\text{C}$ and the salt content of the ice is similar to that of modern first-year sea ice.

Frozen seawater also accretes to the base of Antarctic ice shelves [*Morgan, 1972; Lange and MacAyeal, 1986*], by means of the “ice pump” mentioned above. It is called “marine ice” to distinguish it from “sea ice” forming at the ocean surface; these two forms of frozen seawater differ substantially in their composition and structure. Marine ice forms at a depth of 400 m or so, where the solubility of air in water is greater than at the sea surface, so the ice does not incorporate bubbles. Nor does it contain brine inclusions; its salinity is typically one-thousandth that of seawater [*Warren et al., 1993b, Table 1*], in contrast to sea ice whose salinity is initially about one-third that of seawater. Reasons for the desalination of marine ice were investigated theoretically by *Tabraham [1997]*.

Marine ice at the base of the Amery Ice Shelf attains a thickness of 190 m in places [*Fricke et al., 2001*]; i.e., about 40% of the total ice thickness. Icebergs originating from such ice shelves may capsize, and then the marine ice becomes exposed to view. Its color may be green or blue, depending on the concentration of dissolved organic matter in the ice. Although the ice is bubble-free, it contains a lattice of cracks perpendicular to the surface with a typical spacing of 0.5 m. Their mechanism of formation has not been studied; presumably they result from thermal and/or mechanical stresses. These cracks are responsible for the albedo of marine ice shown in Figure 8. The allwave albedo under the ambient clear sky was 0.27, but with the cold-atmosphere solar spectrum of Figure 2 it would be 0.25 (Table 1).

If the ice on the snowball ocean is hundreds of meters thick, the lower part of the ice sheet may therefore resemble marine ice rather than sea ice. The accreted ice would slowly move upward as the surface is ablated by sublimation and the marine ice might then be exposed at the surface. The development of thermal and mechanical stresses would be much slower than in a capsizing iceberg and the stresses might be released by recrystallization, so the density of cracks might be less.

We adjust the effective bubble density n_{eff} in our radiative transfer model to match the spectral albedos in Figure 8 as closely as possible; the best fit for sea ice is $n_{eff} = 2 \text{ mm}^{-3}$. In the case of marine ice these bubbles in the model, $n_{eff} = 0.1 \text{ mm}^{-3}$, are just a proxy for the cracks which actually cause the scattering.

On the snowball ocean, the rate of freezing to the base of the ice would be at most equal to the sublimation rate, i.e. only 1-10 mm/yr, much slower than for modern sea ice or marine ice. At slow freezing rates the bubble density would be less than at rapid freezing rates, according to the laboratory experiments of Carte [1961] and Bari and Hallett [1974]. Those experiments were performed on freshwater ice and obtained bubble densities orders of magnitude smaller than are found in natural sea ice at the same growth rate, so we cannot apply their results quantitatively. However, it does seem possible that even sea ice only a few meters thick could be as clear as marine ice if it could grow sufficiently slowly in a calm (wave-free) environment.

However, there are two reasons to think that marine ice is unlikely to be exposed at the surface of the snowball ocean. First, the flow of sea-glaciers is sufficiently fast that *Goodman and Pierrehumbert* [2002] predict glacier ice to be exposed even at the equator.

Second, if frozen seawater does sublimate at the equator, a salt crust would likely develop on the surface [Warren *et al.*, 2002].

4.3 Melting sea ice

In the Arctic Ocean, bare multi-year sea ice is exposed in summer after the snowcover has melted and drained. This ice has a high albedo of 0.63 because it is actively melting and develops a granular surface layer that is similar in appearance to coarse-grained snow. This mechanism would be absent if the air temperatures are below freezing throughout the year, but could become important in summer as the climate warms toward the end of a snowball event.

5. Equilibrium ice thickness

Figure 9 shows the equilibrium ice thickness obtained by the spectral model as a function of n_{eff} (top scale) or albedo (bottom scale) for various specified surface temperatures. All curves are for the same incident solar flux, $S_0 = 320 \text{ W m}^{-2}$, but that flux is allowed to impinge on the ice at two different zenith angles. On the Equator at equinox, the daily average insolation-weighted (i.e. cosine-weighted) zenith angle is 38° ; the daily-average penetration-weighted (i.e. secant-weighted) zenith angle is 50° ; both are between the extremes used for Figure 9, which are the global average zenith angle of 60° and the noontime equatorial equinoctial value of 0° .

If we take the plots for $T_s = -30^\circ\text{C}$ as representative of the Snowball Equator, then choosing $n_{eff} = 2 \text{ mm}^{-3}$ (characteristic of sea ice) results in thick ice, whereas $n_{eff} = 0.1 \text{ mm}^{-3}$ (characteristic of marine ice) results in thin ice. (As in the discussion of

Figure 7, we think the lower branch of each of these curves would vanish in a coupled sea-ice/climate model.) To investigate the possibility of photosynthesis at the base of the ice, we compute the penetration of photosynthetically active radiation (PAR; 400-700 nm wavelength) into the ice, assuming overhead Sun (to get the maximum possible transmittance). Photosynthesis is insufficient to support metabolism at light levels below 5×10^{-6} of full sunlight [Raven *et al.*, 2000]. Contours of transmitted PAR shown in Figure 10 indicate that photosynthesis will not occur for an ice thickness greater than about 100 meters even for an albedo as low as 0.17. We then survey all combinations of surface temperature, solar radiation, and albedo that are capable of maintaining 100-m-thick ice (Figure 11). For example, for $S_0 = 320 \text{ W m}^{-2}$ and $\theta_o = 60^\circ$, maintaining thick ice if $\alpha = 0.47$ requires only $T_s < -16^\circ\text{C}$, but for $\alpha = 0.28$, $T_s < -100^\circ\text{C}$ is required.

In assessing the possibility of photosynthesis beneath the ice, the solar zenith angle θ_0 enters the computation in four different ways:

- (a) The incident solar flux is proportional to $\cos \theta_0$.
- (b) The surface albedo increases with θ_0 , particularly for a flat ice surface, for which the reflectance contains a large specular component.
- (c) The zenith angle determines the absorption-attenuation length (h) of the light, which affects the ice thickness. If there are no bubbles then h is just inversely proportional to $\sec \theta_0$.
- (d) For a given ice thickness, the transmittance to water beneath the ice depends on θ_0 .

6. Parameterization of broadband attenuation length

Climate models cannot normally afford to compute radiative transfer in ice at 60 wavelengths, so the broadband approximation (3) is attractive if it can be made accurate. This is possible if we allow h to be a function of bubble content (or broadband albedo). For each ice type (as defined by its bubble-density), an effective broadband h can be chosen that gives the correct thickness Z when used in (2) via (3). Using the spectral model, we determined the equilibrium thickness for a variety of cases (albedos 0.05-0.83, surface temperatures -10 to -60°C , incident solar fluxes 120 - 320 W m^{-2} , and geothermal plus latent heat fluxes 0.04 - 3.40 W m^{-2}), and in each case found the value of h that gave the same thickness. These h -values were fitted by a simple function of the broadband albedo α :

$$h(\alpha) = -2.683 + 20.02 \exp(-10.83\alpha) + 2.742 \exp(-0.03451\alpha), \quad (7)$$

where h is in meters. The albedo α here is a surrogate for bubble density, as given in Figure 5 for the case $Z = 200 \text{ m}$, $\theta_o = 60^\circ$. The effective attenuation length is then $h = 12 \text{ m}$ at $\alpha = 0.05$, decreasing to $h = 0.02 \text{ m}$ at $\alpha = 0.64$ (Figure 12). Equation 7 is valid for albedos 0.05-0.64. For higher albedos (i.e., snow) the computed ice thickness is insensitive to h ; we recommend a constant value, $h = 0.02 \rho_{ice}/\rho_{snow}$, where ρ_{snow} is the density of snow and $\rho_{ice} = 917 \text{ kg m}^{-3}$ (dashed line in Figure 12).

The parameterization gives accurate ice thicknesses for $Z > 40 \text{ m}$ (Figure 13a), but underestimates ice thickness for thin ice (Figure 13b). The errors occur near the inflection points of Figure 9. We found it impossible to derive a parameterization (as a function of the single variable α) that gives accurate ice thickness for thin ice under all heat-flux

conditions, so we chose a parameterization that would give accurate thicknesses for thick ice (i.e. above the inflection points of Figure 9).

This parameterization for h is designed to give accurate thicknesses only; it cannot be expected to give accurate temperatures $T(z)$ within the ice [*Brandt and Warren, 1993, Figure 6*].

7. Accumulation of surface deposits

So far we have assumed that surface deposits are absent. In reality, we can expect (a) patchy snow at times, (b) frost on the surface in the morning or at other times when the surface heat balance is negative, (c) an evaporite accumulation of salt, (d) wind-blown dust from unglaciated continental deserts, and perhaps (e) an evaporite accumulation of freeze-dried algae incorporated into the ice base and carried upward as sublimation proceeds, if photosynthetic life does exist below the ice.

Probably the most important surface deposits are patchy snow and frost; they can dramatically raise the albedo (Figure 8). Another possibly important process is accumulation of salt. The first ice to form on the tropical ocean would probably form quickly, so it should resemble modern sea ice forming in winter. First-year sea ice at the end of winter contains about 0.4% salt [*Cox and Weeks, 1974; 1988*], so about 1 cm of salt would accumulate at the surface if the top 2.5 m of ice sublimates. If the salt is somehow removed, for example by wind, and desalinated marine ice reaches the surface, salt will continue to accumulate, because marine ice does still contain 20 ppm of salt. The consequences of salt accumulation are investigated further by *Warren et al. [2002]*.

The accumulation of freeze-dried algae at the surface, blocking the sunlight so as to suppress photosynthesis below the ice, is also an interesting possibility. It would be an example of life altering its environment in a way that makes it unsuitable for life; i.e. the opposite of Gaia.

8. Discussion and Conclusion

The solution for ice thickness is strikingly bimodal. Low surface temperature T_s , small basal freezing rate F_L , and high albedo α result in equilibrium ice thickness on the order of 1 km. As any of these variables changes in the direction favoring thinner ice, a sharp transition is experienced to equilibrium thicknesses of a meter or less.

Thin ice (~1 m) is common on today's high-latitude oceans because warmer ocean water flowing below the ice supplies a heat flux of several watts per square meter. This source of heat ultimately comes from absorption of sunlight at the sea surface at lower latitudes; it would be absent on the Snowball Earth after completion of a transient period of a few thousand years during which the ocean would lose its reservoir of heat. The existence of widespread thin ice on the modern oceans is therefore not a reason to expect thin ice on a snowball ocean.

The albedo of present-day bare sea ice is about 0.5, but rises to 0.75 at temperatures below -23°C when salts crystallize in the brine pockets. For an albedo of 0.5, and an expected equatorial solar flux of 320 W m^{-2} at the surface of Snowball Earth, we find that surface temperatures below -12°C generate ice layers too thick for photosynthesis ($>100\text{m}$). From this point of view, it seems that if the tropics did freeze, the ice would be too thick to allow photosynthesis.

If the ice were to form more slowly than present-day sea ice, it would contain fewer brine inclusions and air bubbles, and would therefore have lower albedo. For $\alpha = 0.4$, the model predicts thin ice for $T_s > -25^\circ\text{C}$. However, if the albedo were as low as 0.4 over the entire tropical ocean, its absorption of sunlight might cause the surface temperature to rise to 0°C , and melt the thin ice layer.

There is a second reason why thin ice is vulnerable on Snowball Earth: invasion of the sea-glaciers. Kilometer-thick ice on the midlatitude and polar oceans would flow equatorward, with velocities of 2 km/year at an unimpeded ice front, according to calculations of *Goodman and Pierrehumbert* [2002], so it would rapidly fill in any regions of thin ice or open water that might otherwise tend to develop in the snowball tropics. Sea-glaciers flowing into the tropics would lose their snow cover by sublimation, exposing bubbly glacier ice of albedo 0.6, for which the equilibrium ice thickness is >100 m for any surface temperature below -8°C .

Any thin ice that were to form on the snowball ocean would therefore be at risk due to both climatic warming caused by its low albedo, and inflow of sea-glaciers. It could avoid the first danger if it covered only a small area, and might avoid the second if it were either landlocked or nearly landlocked, like the Caspian Sea or Black Sea today.

We have shown ice thickness results for various specified surface temperatures, but have focused our discussion on the results for an equatorial surface temperature of -30°C , the temperature expected during the coldest early part of a snowball event, before the atmospheric CO_2 content had risen substantially to warm the tropics. Our reason for this focus is that this period of a million years or so early in a snowball event would be the most difficult for the survival of photosynthetic life. If the climate model's equatorial

temperature of -30 to -35°C is correct, our results show that a refuge for photosynthetic organisms under widespread thin ice is unlikely, so the survival of photosynthetic eukaryotes most likely would have occurred in small isolated refuges of higher-than-average geothermal heat flux on islands or coastlines.

Acknowledgments. We thank David Pollard for results of his GCM simulations of Snowball Earth, Jason Goodman for pointing out the importance of sea-glacier flow, Kurt Woschnagg for prepublication measurements of the spectral absorption coefficient of ice, and Paul Hoffman and Adam Maloof for discussions. The albedo measurements on sea ice and marine ice were made on expeditions of the Australian Antarctic Division, in collaboration with Ian Allison. Adam Maloof provided helpful comments on the manuscript, and Melanie Fitzpatrick coined the term “sea-glacier.” This research was supported by the National Science Foundation under Grant OPP-98-15156.

References

- Allison, I., R.E. Brandt, and S.G. Warren, East Antarctic sea ice: albedo, thickness distribution and snow cover. *J. Geophys. Res.*, 98, 12417-12429, 1993.
- Askebjerg, P., S.W. Barwick, L. Bergström, A. Bouchta, S. Carius, E. Dalberg, B. Erlandsson, A. Goobar, L. Gray, A. Hallgren, F. Halzen, H. Heukenkamp, P.O. Hulth, S. Hundertmark, J. Jacobsen, V. Kandhadai, A. Karle, I. Liubarsky, D. Lowder, T. Miller, P. Mock, R. Morse, R. Porrata, P.B. Price, A. Richards, H. Rubinstein, E. Schneider, Ch. Spiering, O. Streicher, Q. Sun, Th. Thon, S. Tilav, R. Wischnewski, C. Walck, and G. Yodh, UV and optical light transmission properties in deep ice at the South Pole, *Geophys. Res. Lett.*, 24, 1355-1358, 1997a.
- Askebjerg, P., S.W. Barwick, L. Bergström, A. Bouchta, S. Carius, E. Dalberg, K. Engel, B. Erlandsson, A. Goobar, L. Gray, A. Hallgren, F. Halzen, H. Heukenkamp, P.O. Hulth, S. Hundertmark, J. Jacobsen, A. Karle, V. Kandhadai, I. Liubarsky, D. Lowder, T. Miller, P. Mock, R.M. Morse, R. Porrata, P.B. Price, A. Richards, H. Rubinstein, E. Schneider, Ch. Spiering, O. Streicher, Q. Sun, Th. Thon, S. Tilav, R. Wischnewski, C. Walck, and G.B. Yodh, Optical properties of deep ice at the South Pole: absorption, *Appl. Opt.*, 36, 1168-4180, 1997b.
- Bari, S.A., and J. Hallett, Nucleation and growth of bubbles at an ice-water interface. *J. Glaciol.*, 13, 489-523, 1974.
- Bintanja, R., On the glaciological, meteorological, and climatological significance of Antarctic blue ice areas, *Rev. Geophys.*, 37, 337-359, 1999.
- Bohren, C.F., Colors of snow, frozen waterfalls, and icebergs, *J. Opt. Soc. Am.*, 73, 1646-1652, 1983.

- Brandt, R.E., and S.G. Warren, Solar heating rates and temperature profiles in Antarctic snow and ice. *Journal of Glaciology*, 39, 99-110, 1993.
- Brandt, R.E., C.S. Roesler, and S.G. Warren, Spectral albedo, absorptance, and transmittance of Antarctic sea ice, *Fifth Conference on Polar Meteorology and Oceanography*, American Meteorological Society, Boston, 456-459, 1999.
- Budd, W.F., M.J. Corry, and T.H. Jacka, Results from the Amery Ice Shelf Project, *Ann. Glaciol.*, 3, 36-41, 1982.
- Budyko, M.I., The effect of solar radiation variations on the climate of the earth, *Tellus*, 21, 611-619, 1969.
- Caldeira, K., and J.F. Kasting, Susceptibility of the early Earth to irreversible glaciation caused by carbon dioxide clouds, *Nature*, 359, 226-228, 1992.
- Carte, A.E., Air bubbles in ice, *Proceedings of the Physical Society (London)*, 77, 757-768, 1961.
- Chylek, P., and J.A. Coakley Jr, Analytical analysis of a Budyko-type climate model, *J. Atmos. Sci.*, 32, 675-679, 1975.
- Cox, G.F.N., and W.F. Weeks, Salinity variations in sea ice, *J. Glaciol*, 13, 109-120, 1974.
- Cox, G.F.N., and W.F. Weeks, Numerical simulations of the profile properties of undeformed first-year sea ice during the growth season, *J. Geophys. Res.*, 93, 12449-12460, 1988.
- Evans, D.A.D., Stratigraphic, geochronological, and paleomagnetic constraints upon the Neoproterozoic climatic paradox, *Am. J. Science*, 300, 347-433, 2000.
- Fricker, H.A., S. Popov, I. Allison, and N. Young, Distribution of marine ice beneath the Amery Ice Shelf, East Antarctica, *Geophys. Res. Lett.*, 28, 2241-2244, 2001.

- Goodman, J., and R.T. Pierrehumbert, Glacial flow of floating marine ice in 'Snowball Earth,' submitted to *J. Geophys. Res.*, 2002.
- Grenfell, T.C., A theoretical model of the optical properties of sea ice in the visible and near infrared, *J. Geophys. Res.*, 88, 9723-9735, 1983.
- Grenfell, T.C., and D.K. Perovich, Radiation absorption coefficients of polycrystalline ice from 400 to 1400 nm, *J. Geophys. Res.*, 86, 7447-7450, 1981.
- Grenfell, T.C., and D.K. Perovich, Spectral albedos of sea ice and incident solar irradiance in the southern Beaufort Sea, *J. Geophys. Res.*, 89, 3573-3580, 1984.
- Harland, W.B., Critical evidence for a great Infra-Cambrian glaciation, *Geologische Rundschau*, 54, 45-61, 1964.
- He, Y.D., and P.B. Price, Remote sensing of dust in deep ice at the South Pole, *J. Geophys. Res.*, 103, 17,041-17,056, 1998.
- Hoffman, P.F., and D.P. Schrag, Snowball Earth, *Sci. Am.*, 68(1), 68-75, January 2000.
- Hoffman, P.F., A.J. Kaufman, G.P. Halverson, and D.P. Schrag, A Neoproterozoic Snowball Earth, *Science*, 281, 1342-1346, 1998.
- Kapitsa, A.P., J.K. Ridley, G. deQ. Robin, M.J. Siegert, and I.A. Zotikov, A large deep freshwater lake beneath the ice of central East Antarctica, *Nature*, 381, 684-686, 1996.
- Kennedy, M.J., N. Christie-Blick, and L.E. Sohl, Are Proterozoic cap carbonates and isotopic excursions a record of gas hydrate destabilization following Earth's coldest intervals?, *Geology*, 29, 443-446, 2001.
- Kipfstuhl, J., G. Dieckmann, H. Oerter, H. Hellmer, and W. Graf, The origin of green icebergs in Antarctica, *J. Geophys. Res.*, 97, 20,319-20,324, 1992.

- Kirschvink, J.L., 1992: Late Proterozoic low-latitude global glaciation: the Snowball Earth, in *The Proterozoic Biosphere*, Schopf, J.W., and Klein, C. eds., pp. 51-52, Cambridge Univ. Press, New York, 1992.
- Knoll, A.H., The early evolution of eukaryotes: A geological perspective, *Science*, 227, 57-59, 1985.
- Labs, D., and H. Neckel, Transformation of the absolute solar radiation data into the International Practical Temperature Scale of 1968, *Solar Phys.*, 15, 79-87, 1970.
- Lange, M.A., and D.R. MacAyeal, Numerical models of the Filchner-Ronne Ice Shelf: An assessment of reinterpreted ice thickness distribution, *J. Geophys. Res.*, 91, 10,457-10,462, 1986.
- Lewis, E.L., and R.G. Perkin, Ice pumps and their rates, *J. Geophys. Res.*, 91, 11,756-11,762, 1986.
- Lillie, R.J., *Whole Earth Geophysics*, p. 326, Prentice-Hall, Upper Saddle River, NJ, 1999.
- Maykut, G.A., and N. Untersteiner, Some results from a time-dependent thermodynamic model of sea ice, *J. Geophys. Res.*, 76, 1550-1575, 1971.
- McClatchey, R.A., R.W. Fenn, J.E.A. Selby, F.E. Volz, and J.S. Garing, 1972: *Optical Properties of the Atmosphere (Third Edition)*. Air Force Cambridge Research Laboratories report AFCRL-72-0497, 108 pp.
- McKay, C.P., Thickness of tropical ice and photosynthesis on a snowball Earth, *Geophys. Res. Lett.*, 27, 2153-2156, 2000.
- McKay, C.P., G.D. Clow, R.A. Wharton Jr, and S.W. Squyres, Thickness of ice on perennially frozen lakes, *Nature*, 313, 561-562, 1985.

- McKay, C.P., G.D. Clow, D.T. Andersen, and R.A. Wharton Jr, Light transmission and reflection in perennially ice-covered Lake Hoare, Antarctica, *J. Geophys. Res.*, *99*, 20,427-20,444, 1994.
- Morgan, V.I., Oxygen isotope evidence for bottom freezing on the Amery Ice Shelf, *Nature*, *238*, 393-394, 1972.
- Mullen, P.C., and S.G. Warren, Theory of the optical properties of lake ice, *J. Geophys. Res.*, *93*, 8403-8414, 1988.
- Neckel, H., and D. Labs, The solar radiation between 3300 and 12,500 Angstroms, *Solar Phys.*, *90*, 205-258, 1984.
- Perovich, D.K., and J.W. Govoni, Absorption coefficients of ice from 250 to 400 nm, *Geophys. Res. Lett.*, *18*, 1233-1235, 1991.
- Perovich, D.K., and T.C. Grenfell, Laboratory studies of the optical properties of young sea ice, *J. Glaciol.*, *27*, 331-346 (1981).
- Perovich, D.K., T.C. Grenfell, B. Light, and P.V. Hobbs, The seasonal evolution of Arctic sea-ice albedo, *J. Geophys. Res.*, *in press*, 2002.
- Pollard, D., and J.F. Kasting, Coupled GCM-Ice sheet simulations of Sturtian (750-720 Ma) glaciation: When in the Snowball-Earth cycle can tropical glaciation occur? *Eos*, *82*, S8 (2001).
- Pounder, E.R., *The Physics of Ice*, Pergamon, 151 pp., 1965.
- Price, P.B., and L. Bergström, Optical properties of deep ice at the South Pole: scattering, *Appl. Opt.*, *36*, 4181-4194.
- Ragotzkie, R.A., and G.E. Likens, The heat balance of two Antarctic lakes, *Limnol. Oceanog.*, *9*, 412-425, 1964.

- Raven, J.A., J.E. Kübler, and J. Beardall, Put out the light, and then put out the light. *J. Mar. Biol. Assn. U.K.*, 80, 1-25, 2000.
- Schrag, D.P., R.A. Berner, P.F. Hoffman, and G.P. Halverson, On the initiation of a snowball earth. *Geochem. Geophys. Geosystems*, in press, 2002.
- Sellers, W.D., *Physical Climatology*. University of Chicago Press, 272 pp., 1965.
- Sellers, W.D., A global climatic model based on the energy balance of the earth-atmosphere system. *J. Appl. Meteor.*, 8, 392-400, 1969.
- Tabraham, J. *The Desalination of Marine Ice*. Ph.D. Thesis, Cambridge University, 177 pp., 1997.
- Warren, S.G., Optical constants of ice from the ultraviolet to the microwave, *Appl. Opt.*, 23, 1206-1225, 1984.
- Warren, S.G., D. Pollard, and R.E. Brandt, Ocean surfaces on Snowball Earth, to be submitted, 2002.
- Warren, S.G., R.E. Brandt, and R.D. Boime, Blue ice and green ice. *Antarctic Journal of the U.S.*, 28, 255-256, 1993a.
- Warren, S.G., C.S. Roesler, V.I. Morgan, R.E. Brandt, I.D. Goodwin, and I. Allison, Green icebergs formed by freezing of organic-rich seawater to the base of Antarctic ice shelves. *J. Geophys. Res. (Oceans)*, 98, 6921-6928 and 18309, 1993b.
- Warren, S.G., C.S. Roesler, and R.E. Brandt, Solar radiation processes in the East Antarctic sea ice zone. *Antarctic J. U.S.*, 32, 185-187, 1997.
- Wettlaufer, J. S., Introduction to Crystallization Phenomena in sea ice, in *Physics of Ice-Covered Seas*, edited by M. Leppäranta, University of Helsinki Press, 105-194, 1998.

Williams, G., and P. Schmidt, Proterozoic equatorial glaciation: Has 'snowball earth' a snowball's chance?, *Australian Geologist*, 117, 21-25, 2000. [Reply by P.F. Hoffman, <<http://www.eps.harvard.edu/people/faculty/hoffman/TAG.html>>]

Wiscombe, W.J., R.M. Welch and W.D. Hall, The effects of very large drops on cloud absorption, Part I, Parcel models, *J. Atmos. Sci.*, 41, 1336-1355, 1984.

Author Addresses

R.E. Brandt, T.C. Grenfell, and S.G. Warren, Department of Atmospheric Sciences, Box 351640, University of Washington, Seattle, WA 98196-1640 (email: brandt@atmos.washington.edu; tcg@atmos.washington.edu; sgw@atmos.washington.edu)

C.P. McKay, Space Science Division, Mail Stop 245-3, Moffett Field, CA 94035 (email: cmckay@arc.nasa.gov)

Figure captions

Figure 1. Spectral absorption coefficient of pure ice from laboratory measurements [*Grenfell and Perovich, 1981; Perovich and Govoni, 1991; Warren, 1984*], and as inferred from field measurements by the AMANDA project [*Askebjerg et al., 1997a, Figure 4; K. Woschnagg, personal communication, 2002*]. Also shown is the broadband absorption coefficient used for sea ice on Snowball Earth by *McKay [2000]*.

Figure 2. Downward solar spectrum, with solar constant reduced by 6% from its present value, at zenith angle 60° . The spectrum is plotted for the top of the atmosphere [*Labs and Neckel, 1970; Neckel and Labs, 1984*], and at a sea-level surface either under the subarctic summer (SAS) standard atmosphere [*McClatchey et al., 1972*] or under an atmospheric temperature and humidity profile suggested for low latitude in daytime on Snowball Earth: temperatures reduced proportionately from SAS at all levels to give a surface temperature of -40°C , and assuming water-vapor saturation with respect to ice throughout the troposphere (up to 10 km). The spectrally integrated fluxes (in W m^{-2}) are 644 at the top of the atmosphere, 509 at the surface under the subarctic summer atmosphere, and 566 at the surface under the cold atmosphere.

Figure 3. Solar energy absorbed per unit volume (i.e., heating rate) as a function of depth within the top meter of the ice, comparing the broadband model with the spectral model. Number-density of bubbles is $n_{eff} = 10 \text{ mm}^{-3}$, chosen to give albedo 0.60. The incident solar flux of 320 W m^{-2} is thought to represent annual average conditions at the equator of Snowball Earth.

Figure 4. Solar energy absorbed per unit volume, as a function of depth in the top millimeter of the ice, for the spectral model, both for pure bubble-free ice and for ice with a high bubble density.

Figure 5. Spectrally-averaged (“allwave”) albedo as a function of bubble density, for ice thickness $Z = 200 \text{ m}$ or 2 m , and solar zenith angle $\theta_0 = 0^\circ$ or 60° .

Figure 6. Percent of the absorbed solar flux that is absorbed in the topmost 1 mm, 1 cm, or 10 cm of the ice, for two different zenith angles, as a function of bubble density (lower scale) or the corresponding albedo for thick ice (top scale). In the broadband model only 12% of the absorbed sunlight is absorbed in the top 10 cm.

Figure 7. Equilibrium ice thickness predicted by both the spectral and broadband models, as a function of bubble density (top scale) or the corresponding thick-ice albedo (lower scale). All input variables are the same in both models, at values thought appropriate for the equator of Snowball Earth. The only difference between the models is that the penetration depth h and the albedo have constant values for all wavelengths in the broadband model but vary with wavelength in the spectral model. The lower (thin-ice) branch of the curve is artificial, because T_s is fixed at -30°C . For $\alpha < 0.4$ in a coupled sea-ice/climate model, T_s would most likely rise and the ice would melt (dashed line).

Figure 8. Spectral albedos of possible modern surrogates for ocean surfaces on Snowball Earth. The blue glacier ice was measured in the Trans-Antarctic Mountains by *Warren et al.* [1993a]. Sea ice and icebergs were measured near the coast of Antarctica at 68°S , 77°E [*Warren et al.*, 1997]. The sea ice was 1.4 m thick and windswept, so it was mostly bare, but there were patches of thin snowcover covering areas large enough for their albedo to be measured as well (upper curve). The blue marine ice was measured on a capsized iceberg; the ice had originally frozen to the base of an ice shelf. The sub-eutectic sea ice was measured in a laboratory by *Perovich and Grenfell* [1981].

Figure 9. Equilibrium ice thickness from the spectral model, as a function of bubble density (top scale) or of the corresponding thick-ice albedo (bottom scale), for annual average equatorial solar flux entering the ice either vertically or at zenith angle 60° , for seven air temperatures.

Figure 10. Fraction of incident photosynthetically active radiation (PAR; 400-700 nm wavelength) transmitted through the ice, contoured as functions of depth and bubble density (or albedo, top scale), for zenith sun. Bubble densities of blue marine ice and bare sea ice are indicated for reference.

Figure 11. Surface temperature required to obtain ice thickness of 100 m, contoured as functions of incident solar flux and albedo (a surrogate for bubble density), for two different angles of incidence of the sunlight.

Figure 12. Parameterization of the absorption-attenuation length h to be used in the broadband model, as a function of albedo α (Eq. 7). Use of this parameterization permits the broadband model to compute an approximately correct ice thickness. For $\alpha > 0.64$ (snow) we recommend $h = 0.02 \rho_{ice} / \rho_{snow}$, where ρ_{snow} is the density of snow and $\rho_{ice} = 917 \text{ kg m}^{-3}$ (dashed line).

Figure 13. Ice thickness Z computed by the broadband model using parameterized $h(\alpha)$, versus ice thickness computed by the spectral model. The broadband attenuation length h is given by (7). Ice thickness Z is then computed by means of either the implicit Eq. 2 or the explicit Eq. 3 of *McKay et al.* [1985]. The same points are shown in both frames; frame (b) uses a log scale to show the errors for $Z < 100$ m. For $Z < 40$ m only the implicit equation (requiring an iterative solution) is used because the explicit equation gives much larger errors.

Table 1. Potential modern surrogates for equatorial sea ice with no surface deposits.

	Albedo ($\theta_0 = 60^\circ$)	Albedo ($\theta_0 = 0^\circ$)
Cold blue glacier ice [Warren <i>et al.</i> , 1993a]	0.63	
Cold blue glacier ice [Bintanja, 1999, Figure 14]	0.6	0.57 ⁺
Nonmelting snowfree sea ice, $T_s = -5^\circ\text{C}$ [Brandt <i>et al.</i> , 1999]	0.49* (0.47 ⁺)	0.44 ⁺
Sub-eutectic bare sea ice, $T_s = -37^\circ\text{C}$ [Perovich and Grenfell, 1981]	0.75* (0.71 ⁺)	0.69 ⁺
Marine ice [Warren <i>et al.</i> , 1997]	0.27* (0.25 ⁺)	0.21 ⁺
Melting multiyear Arctic sea ice with granular surface layer [Grenfell and Perovich, 1984; Perovich <i>et al.</i> , 2002]	0.63 \pm 0.05	

*Albedos under ambient environmental conditions during the measurement.

⁺Albedos for solar spectrum expected under colder atmosphere (Figure 2).

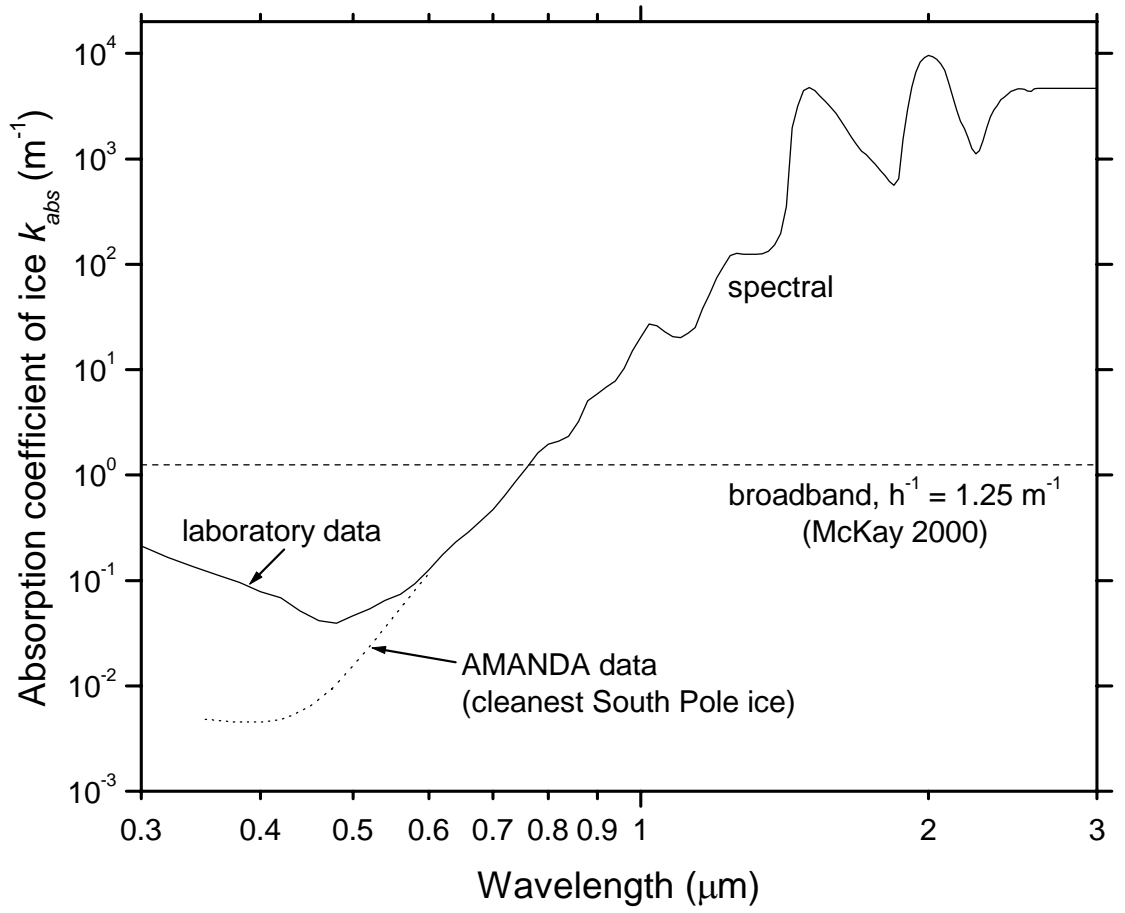


Figure 1

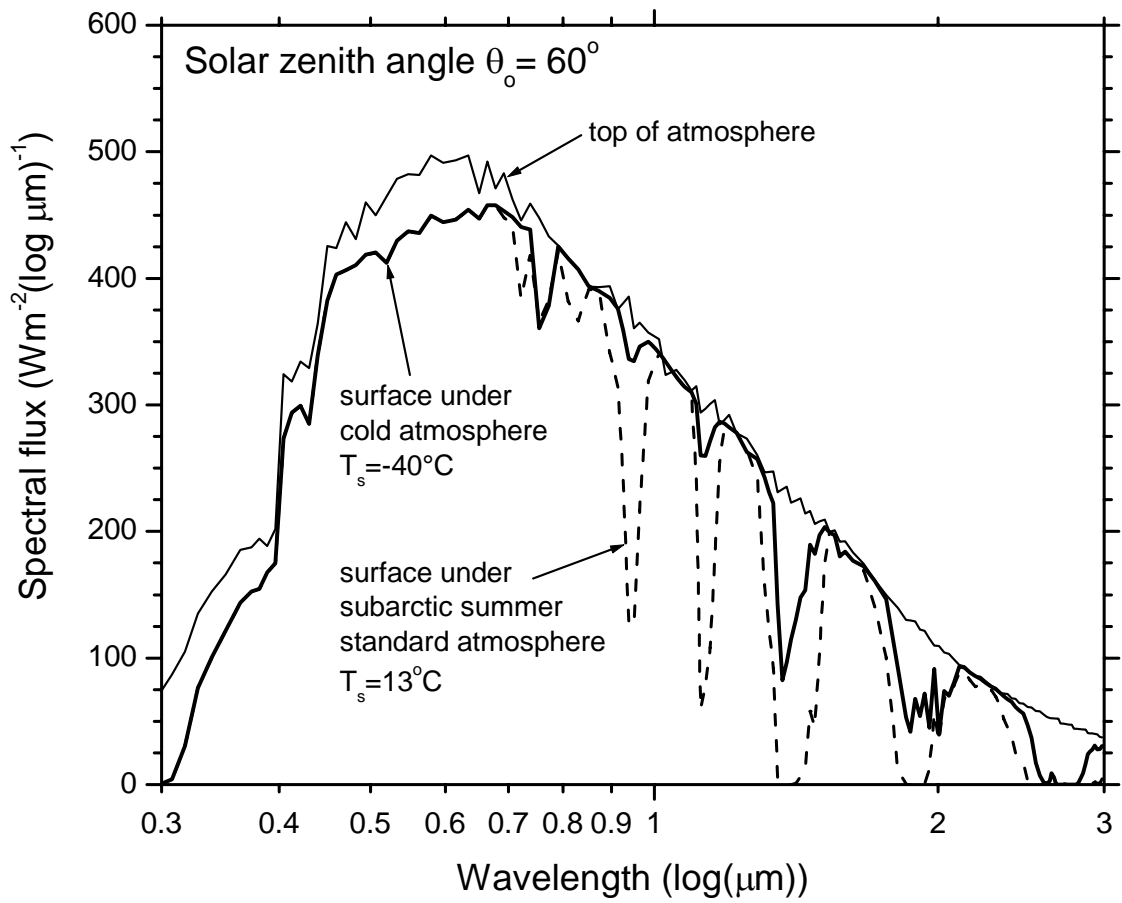


Figure 2

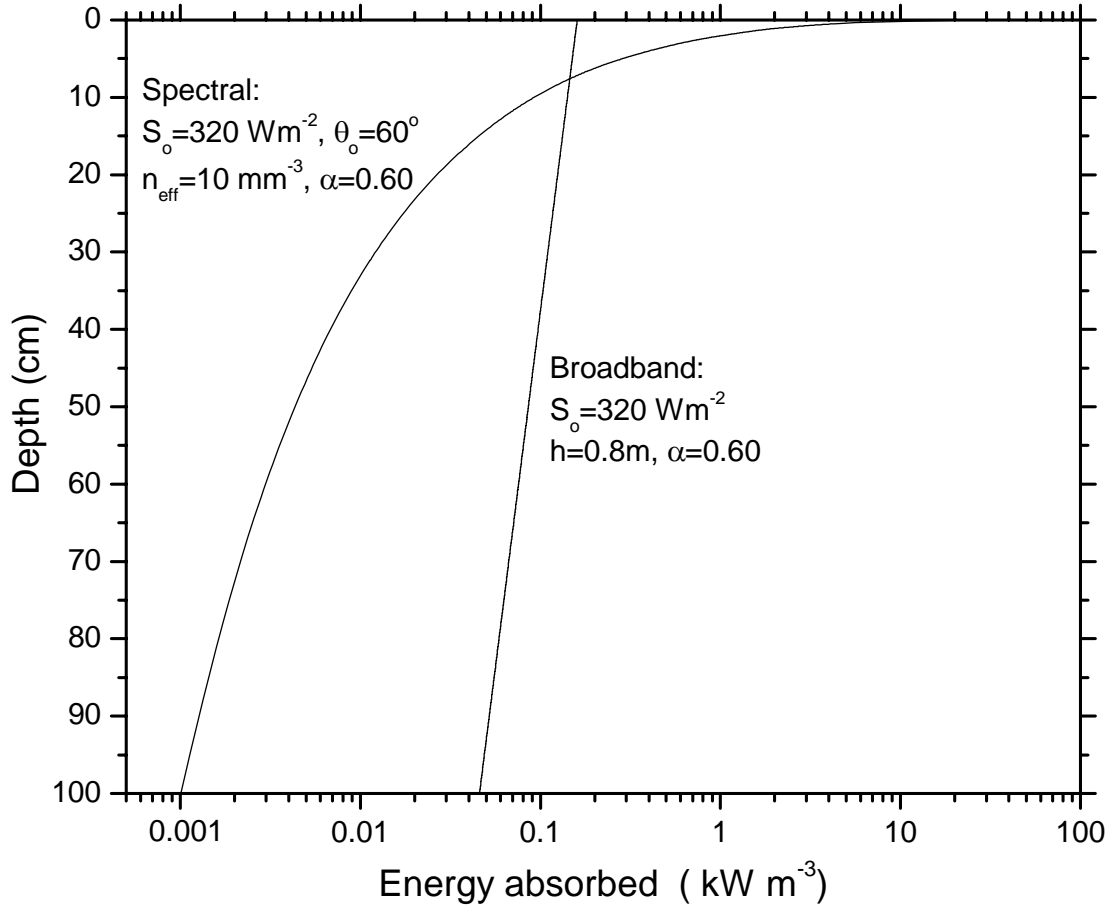


Figure 3

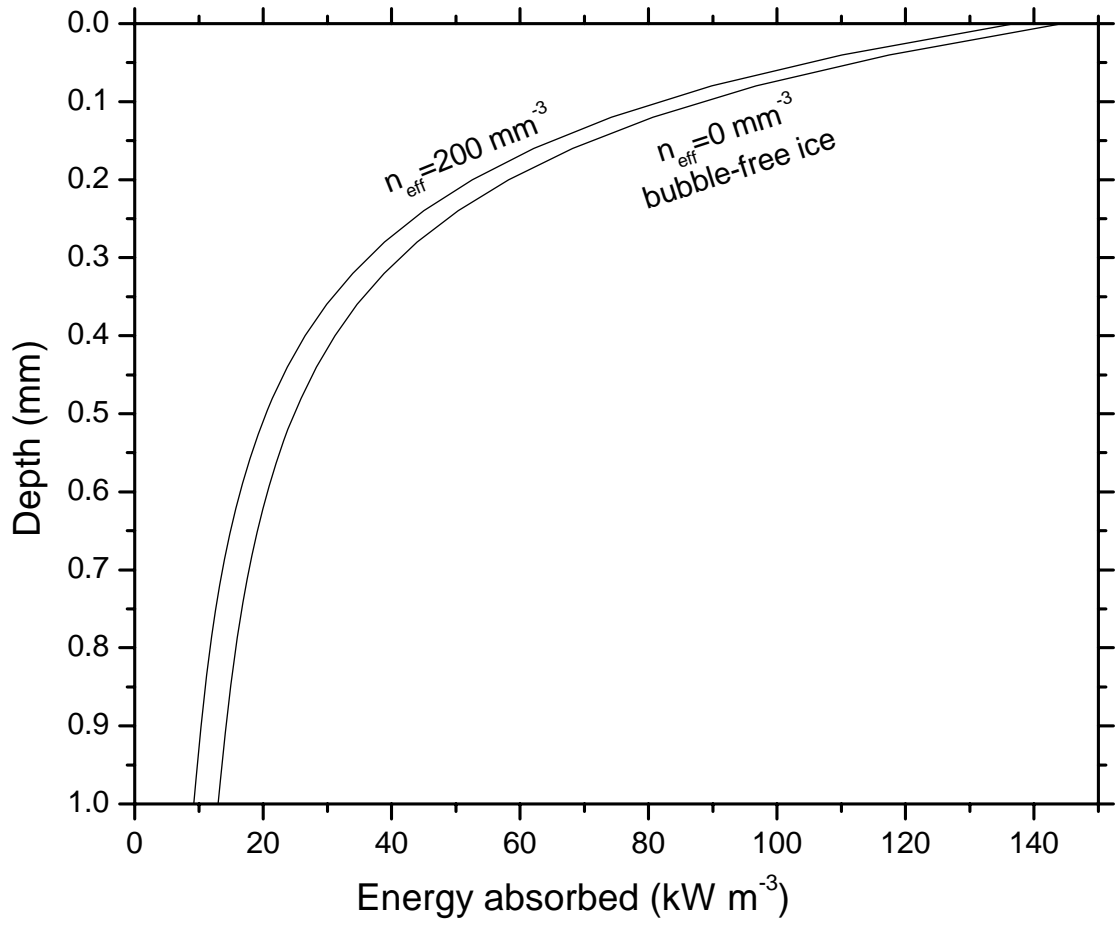


Figure 4

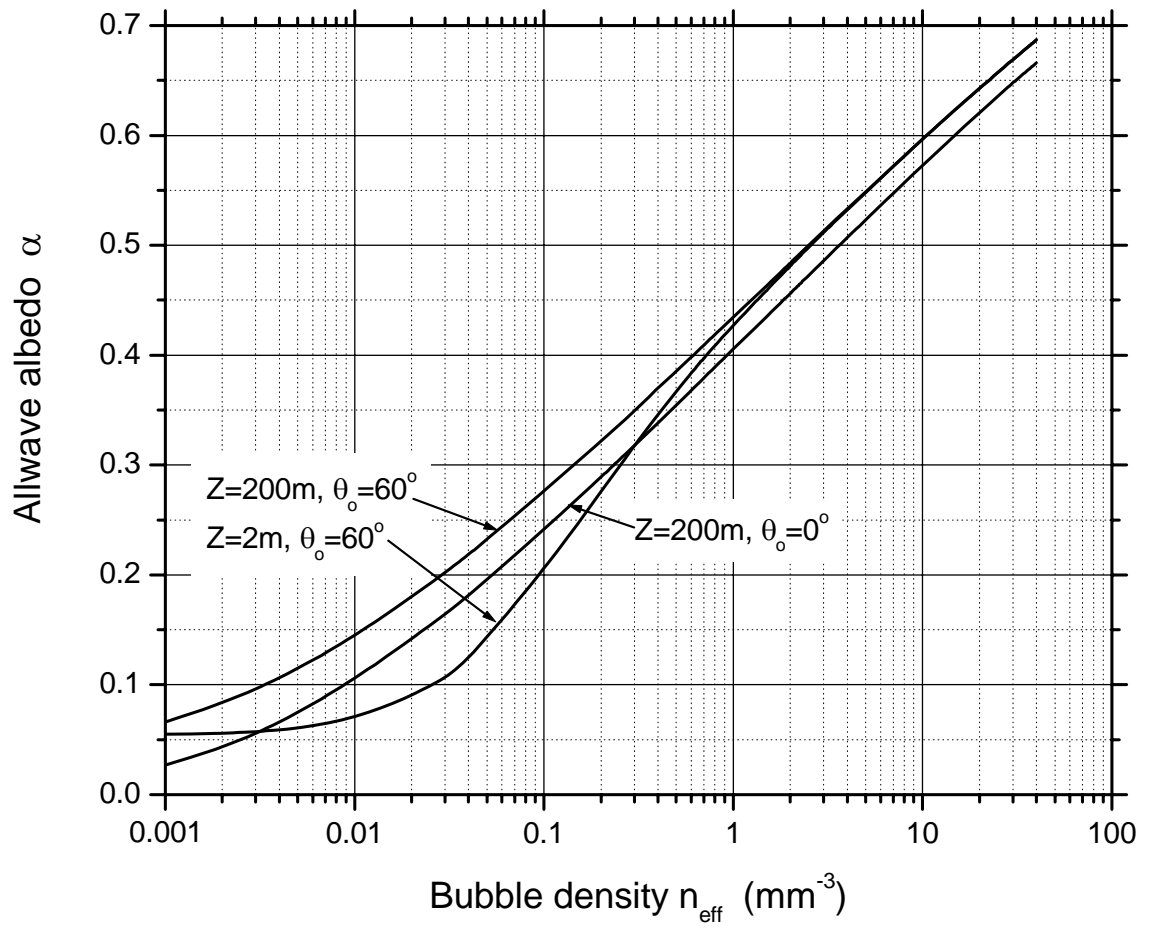


Figure 5

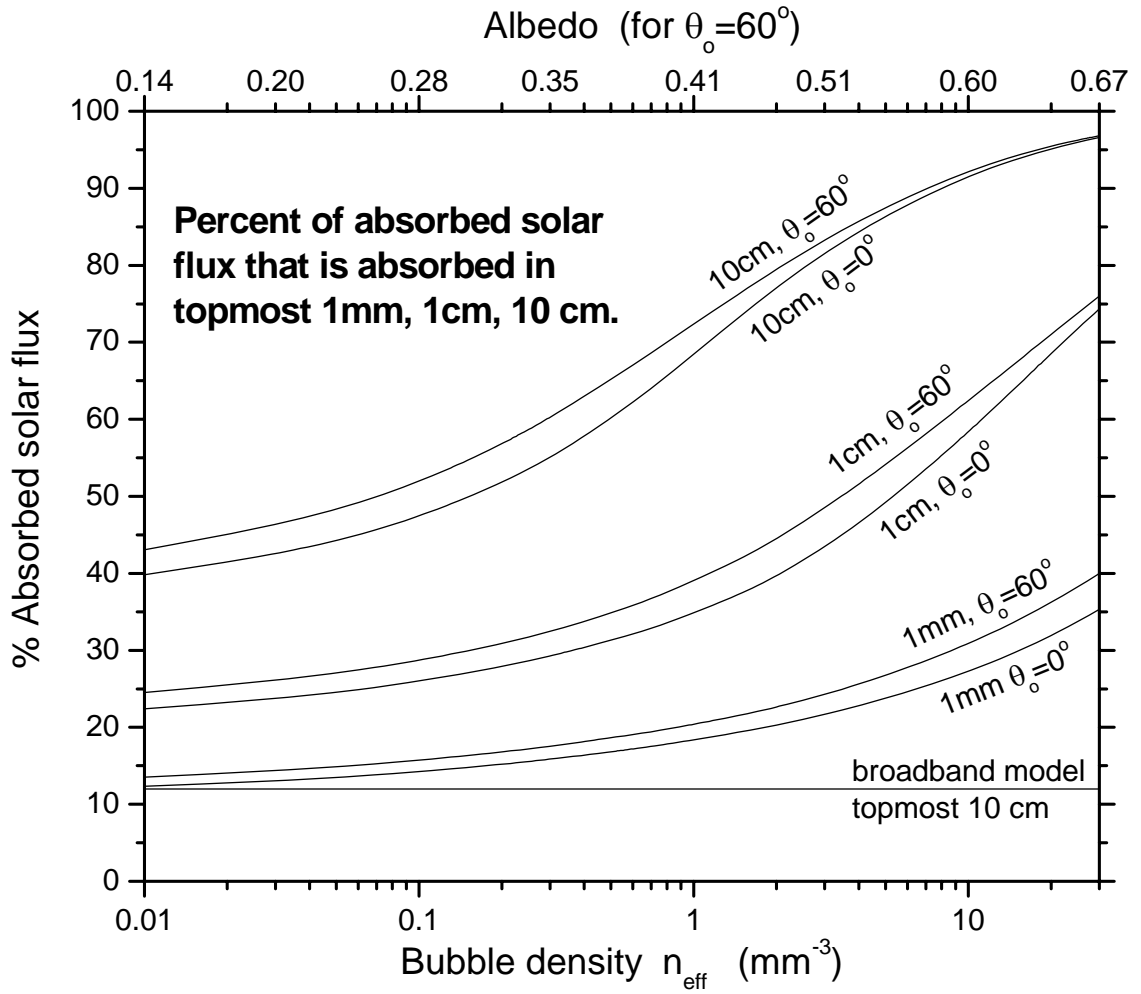


Figure 6

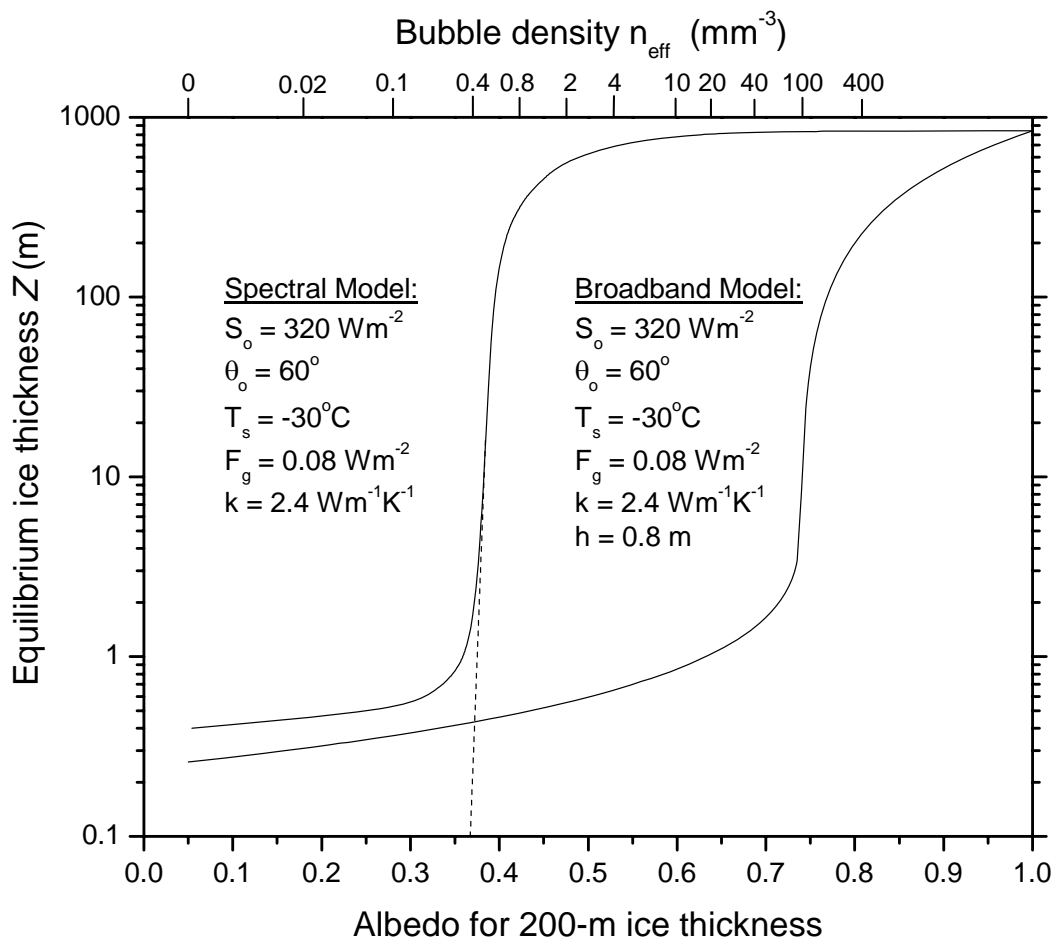


Figure 7

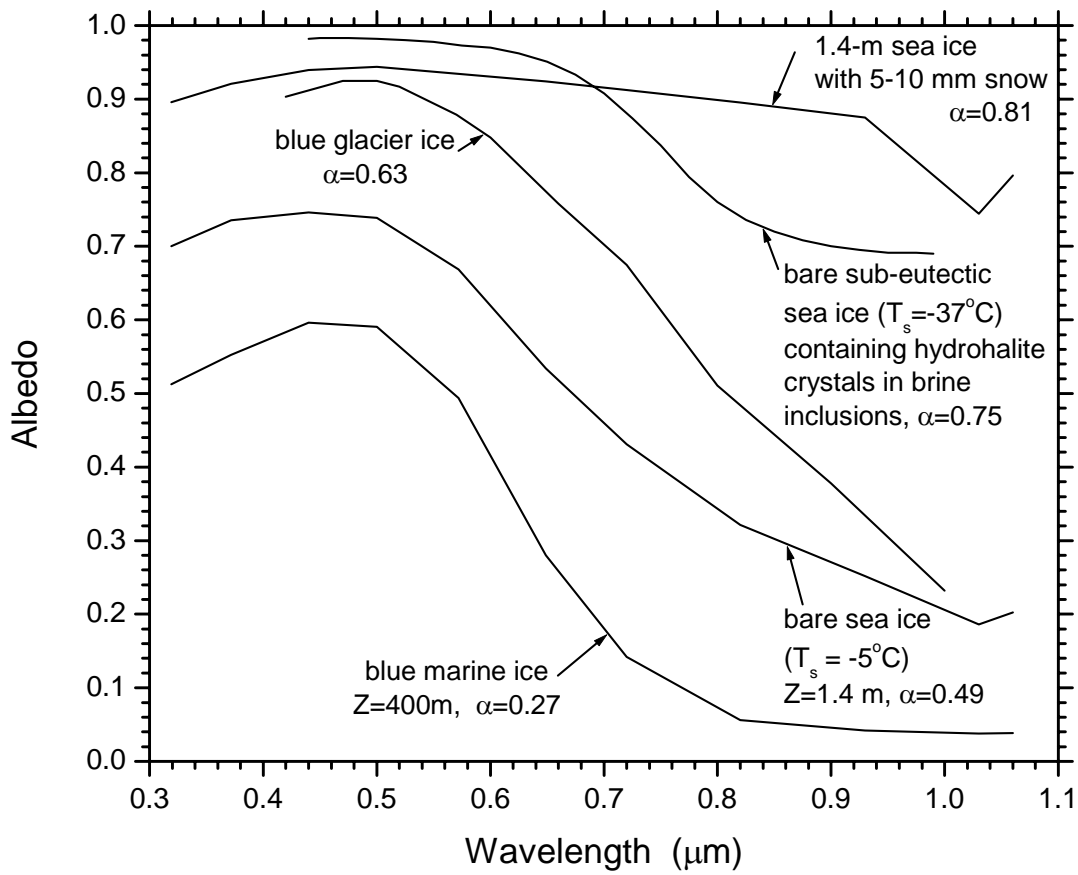


Figure 8

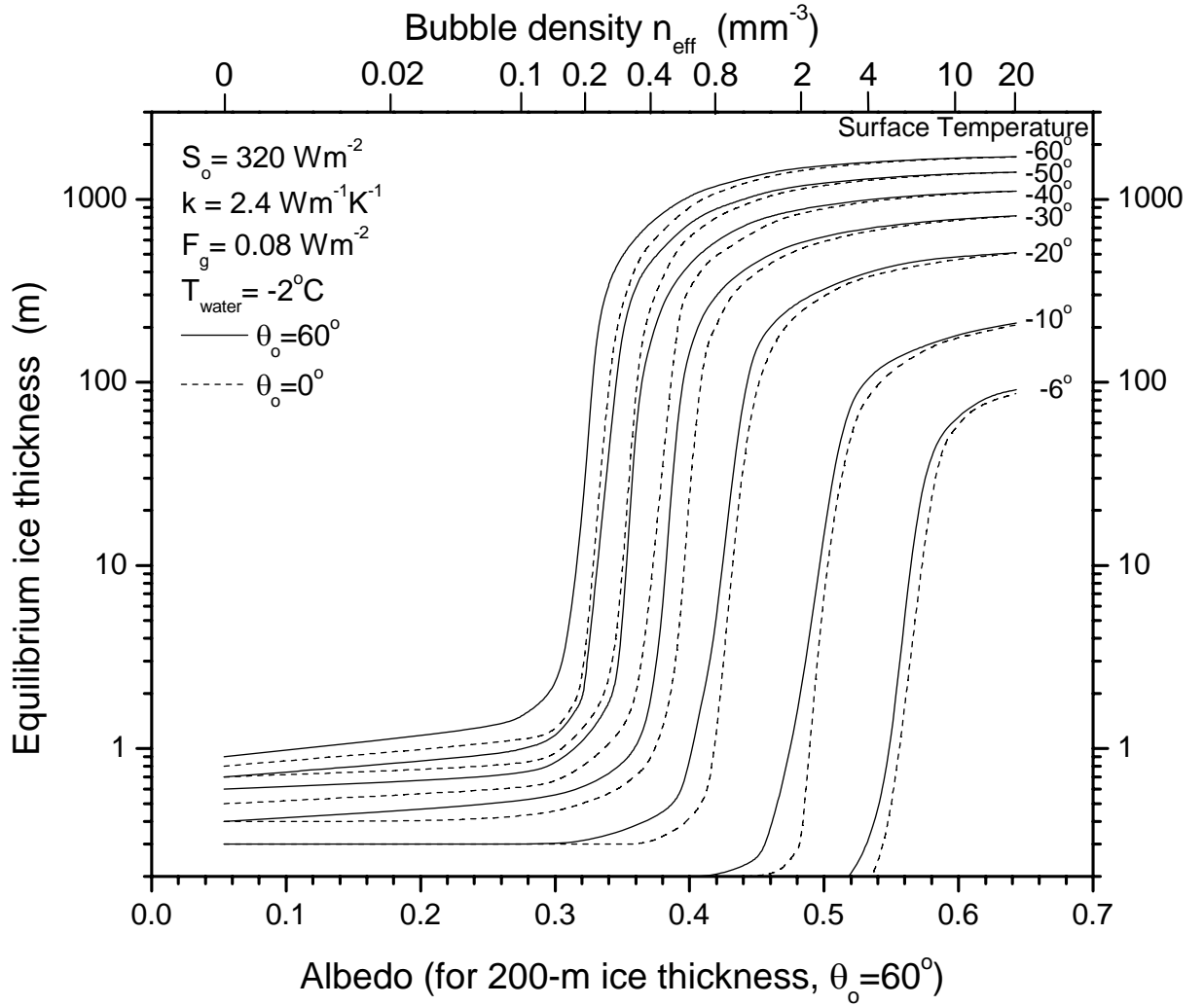


Figure 9

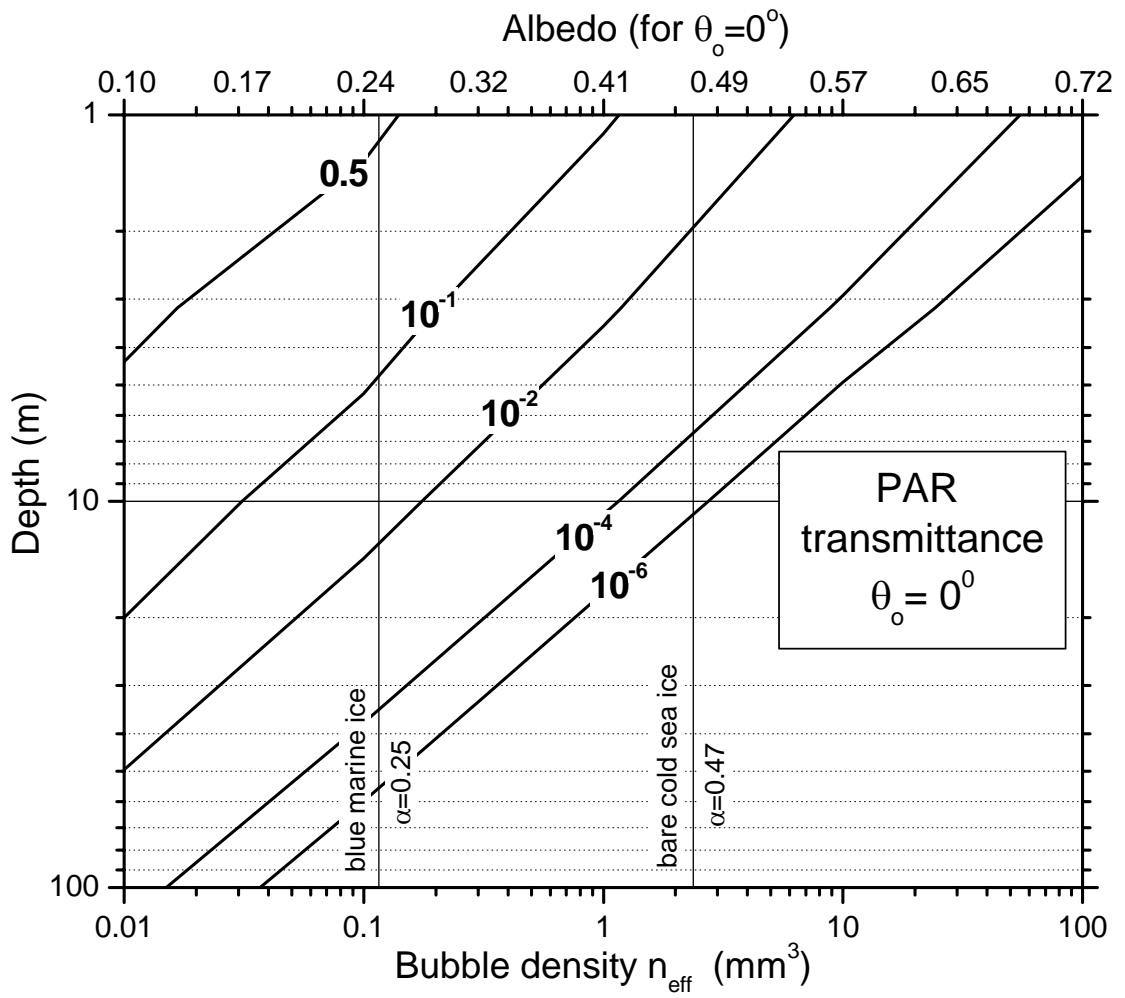


Figure 10

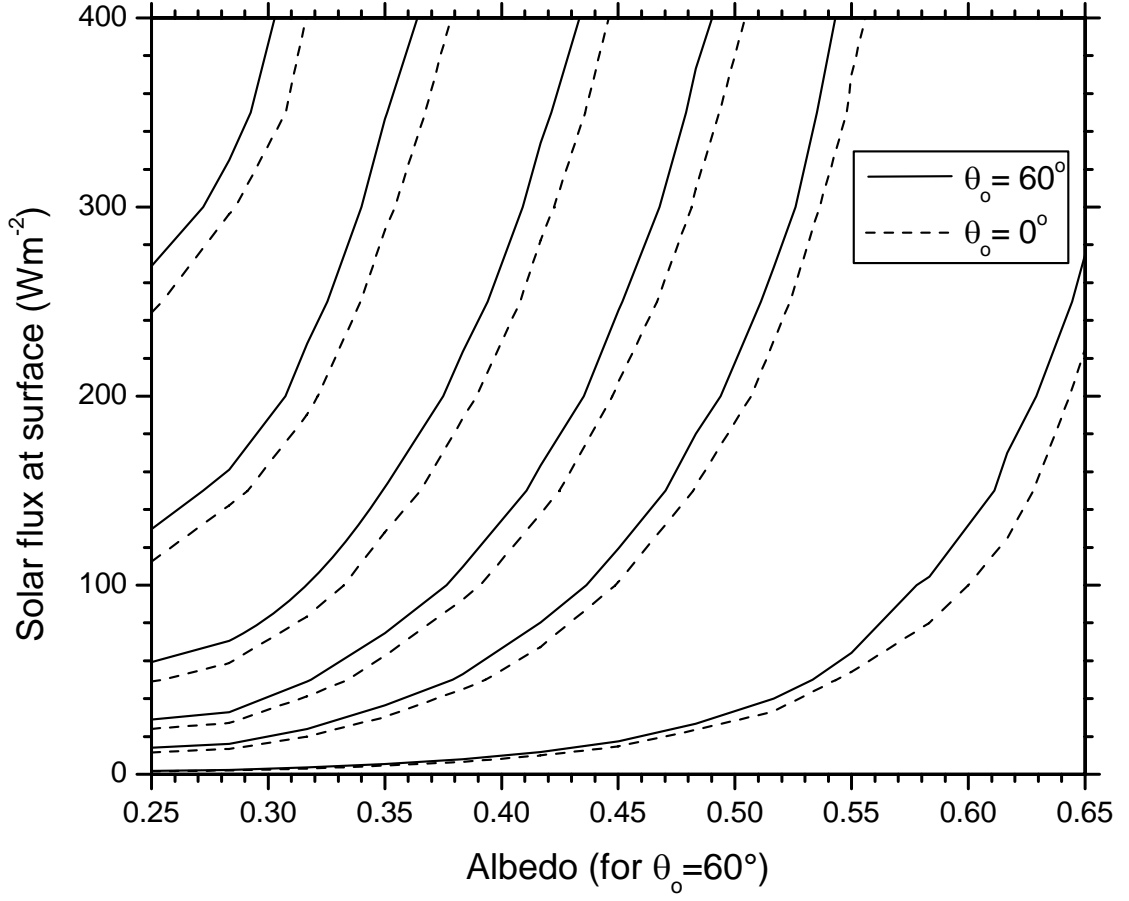


Figure 11

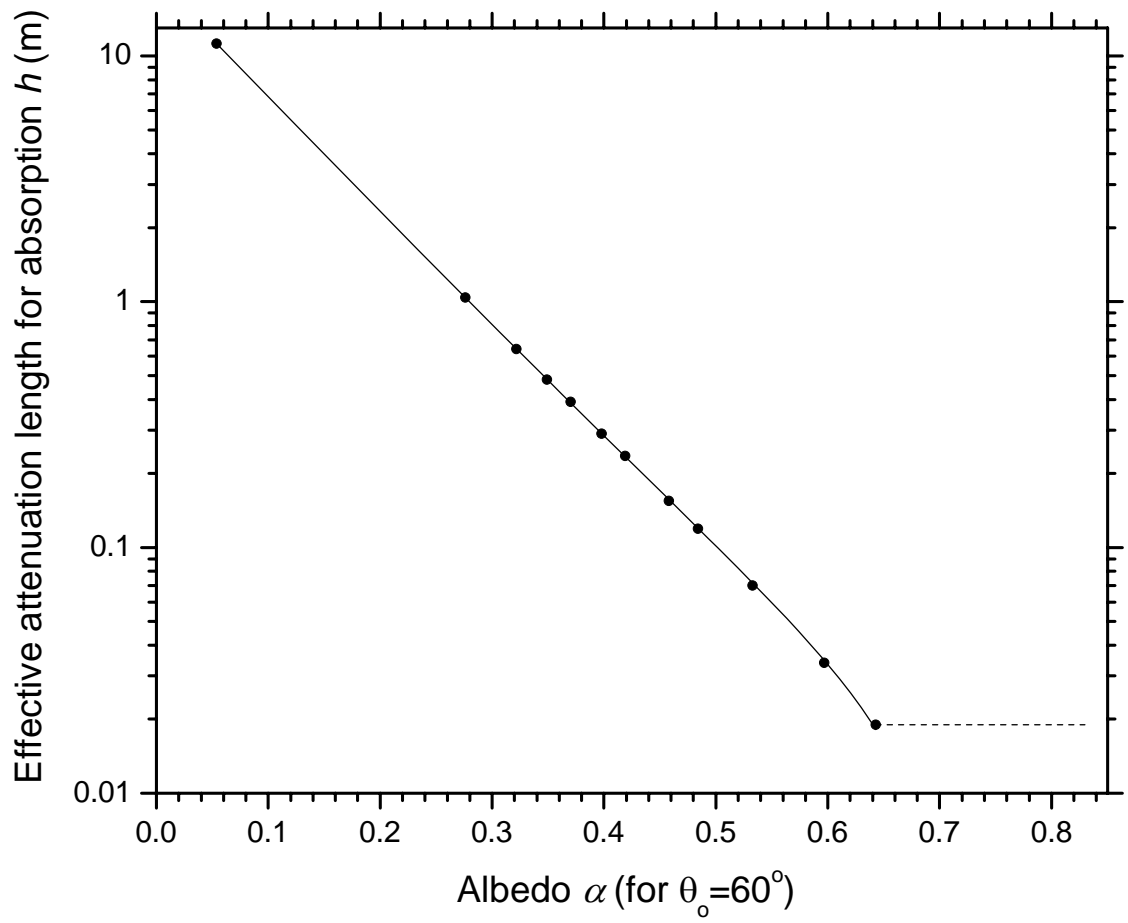


Figure 12

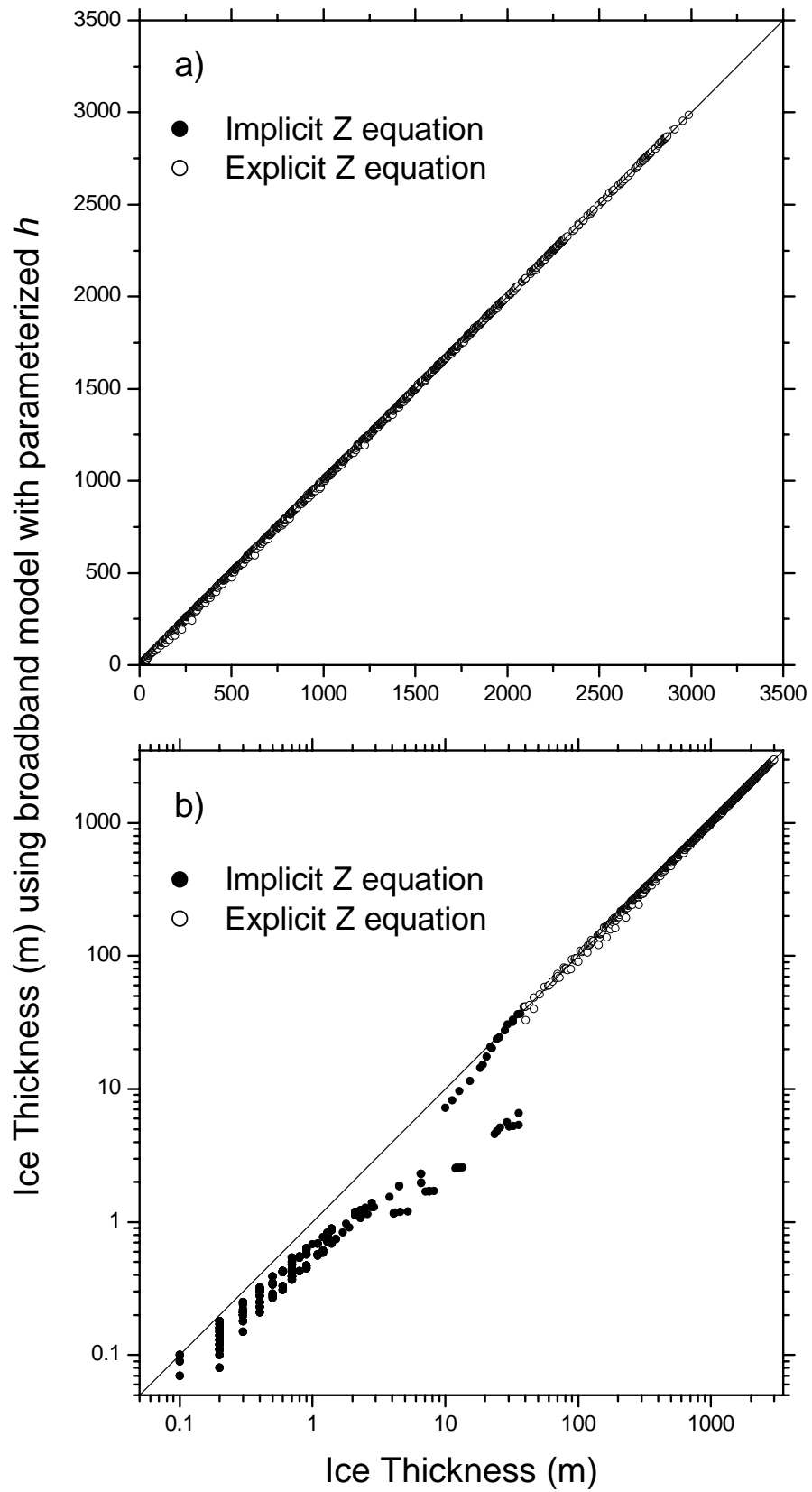


Figure 13